precursor protein mutation, but not a case with presenilin mutation, seemed to show more widespread Aβ plaque-like AQP4 expression than sAD cases. Because of the small number of fAD or sAD cases showing Aβ plaque-like AQP4 expression, we were unable to perform statistical analysis to clarify this issue.

Our present observations suggest that AQP1-expressing astrocytes accumulate at sites of Aβ42 or Aβ40 deposition, where they attempt to take up and degrade the Aβ (26). We consider that during the development of AD pathology, AQP1-expressing astrocytes might contribute, at least temporarily, to a reduction in local SP formation. Although the close relationship between Aβ plaques and microglial cells has been extensively studied, the role of astrocytes in Aβ plaque processing and metabolism is unclear (7, 8, 10, 27). However, it has been suggested that astrocytes have an important role in maintaining Aβ homeostasis in the AD brain. Indeed, large amounts of Aβ have been observed in activated astrocytes in human AD brain (1, 7), and some studies have shown that astrocytes can internalize Aβ both in vitro and ex vivo (6, 9, 11, 27). Furthermore, the amount of Aβ accumulated by astrocytes has been shown to correlate with the severity of AD-associated neuropathology (27), thus strengthening the view that astrocytes are key mediators of Aβ pathology. Although some studies have noted that a subpopulation of activated astrocytes express an Aβ-degrading enzyme that may play a role in Aβ clearance (6, 9, 28), the AQP1-expressing astrocytes demonstrated in the present study might also play a crucial role in SP formation.

In addition, astrocytic AQP1 expression in the AD brain seems to be important for enhancement of astrocyte migration. Cell migration generally involves the formation of membrane protrusions (lamellipodia and membrane ruffles) at the leading edge of the cell. In Chinese hamster ovary cells, exogenously expressed AQP1 is localized at lamellipodia (29), leading to the production of extensive protrusions and accelerated cell migration. Accordingly, it can be hypothesized that the expression of AQP1 observed in our AD cases might play a role in enhancing the ability of astrocytes to migrate toward Aβ plaques. This would also imply that astrocytes might lose their AQP1 expression in the presence of Aβ or other factors in areas with a dense Aβ42 burden. In other words, Aβ42-overburdened astrocytes lacking AQP1 expression might be involved in a process that will result in the formation of astrocyte-derived plaques (7, 30).

In general, although AQP1 is constitutively expressed in the choroid plexus, several studies have demonstrated that astrocytes elsewhere in the brain can express AQP1 under certain pathologic conditions, such as Creutzfeldt-Jacob disease (31), astrocytoma (22), epilepsy (32), and other processes involving astrocytic proliferation (33–36). However, it is still unclear why astrocytic AQP1 expression is upregulated in these disorders when there is no accompanying accumulation of Aβ. Using an Aβ11–25 antibody reactive with both Aβ42 and Aβ40 antigens, Misawa et al (13) have shown that the number of Aβ/AQP1–immunoreactive plaques in AD was significantly higher than in non-AD conditions such as Parkinson disease, multiple-system atrophy, amyotrophic lateral sclerosis, and some other diseases. In AD, increment of Aβ/AQP1–immunoreactive plaques may be a neuropathologic feature that distinguishes it from other neurodegenerative diseases.

Another conspicuous feature in the present study was the expression of AQP4 at SPs or around areas of CAA. Moftakhar et al (14) also studied the distribution of AQP4 plaque-like bodies in human AD brains, but they did not differentiate between Aβ42 and Aβ40 with regard to the respective association of each with AQP4 and did not describe the morphology of AQP4 plaque-like expression in detail. We found that intense Aβ plaque-like expression of AQP4 was closely associated with Aβ42 plaques and that mature SPs involving Aβ40 or dense-cored Aβ plaques lacked internal expression of AQP4. The distribution of AQP4 expression around SPs in the present study suggests that the AQP4 may play a key role in SP formation in AD. It is considered that the amyloid in the cores of classic plaques is older than that in primitive plaques and that the cores are surrounded by a halo of younger amyloid (37). Thus, the expression of AQP4 in SPs seems to occur during early Aβ deposition, whereas AQP4 downregulation seems to occur in the later stage of Aβ plaque formation.

We also noted alterations of AQP4 expression around larger vessels or capillaries affected by CAA; AQP4 expression seemed to vary depending on the severity of CAA. In general, Aβ infiltrates all layers of the vessel wall with progression of CAA, and intracortical vessels including capillaries can show additional spread of Aβ into the surrounding neuropil (so-called dyshoric change) (38, 39). In addition, many studies have shown that vascular Aβ in CAA is predominantly composed of Aβ40 (1, 4, 38), and our findings in CAA in the present series are in accord with those reports. Two studies have reported the changes in AQP4 expression associated with CAA affecting larger vessels (14, 40), and we observed some differences in the distribution of AQP4 immunoreactivity around areas of mild to moderate, or marked, Aβ40 deposition associated with dyshoric change in larger vessels or capillaries. These findings suggest that Aβ-laden blood vessels do interact with astrocytes during CAA progression. In particular, the latter pattern of AQP4 expression around areas of marked Aβ40 deposition is characterized morphologically by glial scar formation (16, 41). In the presence of dyshoric vascular Aβ deposition, clusters of activated microglia and astrocytes have been observed in perivascular areas (39), and upregulation of AQP4 in astrocytes has been found in various inflammatory lesions (42). The inflammatory reaction related to CAA with dyshoric change seems to give rise to enhancement of AQP4 immunoreactivity around areas of CAA.

In summary, we have demonstrated marked changes in the expression of AQP1 and AQP4 in relation to SPs or CAA in human brains affected by AD. Although the number of cases examined was limited, we obtained largely consistent observations that allow us to propose a model for the relationship between AQPs and Aβ. Further studies will be needed to verify the proposed mechanistic link between AQPs and the process of Aβ pathology in AD and to clarify the relationship between AQP-mediated water balance and neurodegenerative process.

ACKNOWLEDGMENT

The authors thank Junko Takasaki and Chieko Tanda for their technical assistance.

REFERENCES

1. Duyckaerts C, Delatour B, Potier MC. Classification and basic pathology of Alzheimer disease. Acta Neuropathol 2009;118:5–36
2. Iwatsubo T, Okada A, Suzuki N, et al. Visualization of Aβ42(43) and Aβ40 in senile plaques with end-specific Aβ monoclonals: Evidence that an initially deposited species is Aβ42(43). Neuron 1994;13:45–53
3. Sgourakis NG, Yan Y, McCallum SA, et al. The Alzheimer's peptides Aβ40 and 42 adopt distinct conformations in water: A combined MD/NMR study. J Mol Biol 2007;368:1448–57
4. Suzuki N, Iwatsubo T, Odaka A, et al. High tissue content of soluble β1–40 is linked to cerebral amyloid angiopathy. Am J Pathol 1994;145: 452–60
5. Mann DM, Pickering-Brown SM, Takeuchi A, et al. Amyloid angiopathy and variability in amyloid β deposition is determined by mutation position in presenilin-1–liked Alzheimer's disease. Am J Pathol 2001;158: 2165–75
6. Koistinaho M, Lin S, Wu X, et al. Apolipoprotein E promotes astrocyte colocalization and degradation of deposited amyloid-β peptides. Nat Med 2004;10:719–26
7. Nagele RG, Wegiel J, Venkataraman V, et al. Contribution of glial cells to the development of amyloid plaques in Alzheimer's disease. Neurobiol Aging 2004;25:663–74
8. Nielsen HM, Mulder SD, Beliën JA, et al. Astrocytic Aβ1–42 uptake is determined by Aβ aggregation state and the presence of amyloid-associated proteins. Glia 2010;58:1235–46
9. Wyss-Coray T, Loike JD, Brionne TC, et al. Adult mouse astrocytes degrade amyloid-β in vitro and in situ. Nat Med 2003;9:453–57
10. Mandybur TI, Chuirazzi CC. Astrocytes and the plaques of Alzheimer's disease. Neurology 1990;40:635–39
11. Verkhratsky A, Olabarria M, Noristani HN, et al. Astrocytes in Alzheimer's disease. Neurotherapeutics 2010;7:399–412
12. Huysseune S, Kienlen-Campard P, Hébert S, et al. Epigenetic control of aquaporin 1 expression by the amyloid precursor protein. FASEB J 2009; 23:4158–67
13. Misawa T, Arima K, Mizusawa H, et al. Close association of water channel AQP1 with amyloid-β deposition in Alzheimer disease brains. Acta Neuropathol 2008;116:247–60
14. Moftakhar P, Lynch MD, Pomakian JL, et al. Aquaporin expression in the brains of patients with or without cerebral amyloid angiopathy. J Neuropathol Exp Neurol 2010;69:1201–9
15. Pérez E, Barrachina M, Rodríguez A, et al. Aquaporin expression in the cerebral cortex is increased at early stages of Alzheimer disease. Brain Res 2007;1128:164–74
16. Badaut J, Ashwal S, Obenaus A. Aquaporins in cerebrovascular disease: A target for treatment of brain edema? Cerebrovasc Dis 2011;31:521–31
17. Badaut J, Lasbennes F, Magistretti PJ, et al. Aquaporins in brain: Distribution, physiology, and pathophysiology. J Cereb Blood Flow Metab 2002;22:367–78
18. Tait MJ, Saadoun S, Bell BA, et al. Water movements in the brain: Role of aquaporin. Trends Neurosci 2008;31:37–43
19. Yool AJ. Aquaporins: Multiple roles in the central nervous system. Neuroscientist 2007;13:470–85
20. Aoki K, Uchihara T, Tsuchiya K, et al. Enhanced expression of aquaporin 4 in human brain with infarction. Acta Neuropathol 2003;106:121–24
21. Hoshi A, Yamamoto T, Shimizu K, et al. Chemical preconditioning-induced reactive astrocytosis contributes to the reduction of post-ischemic edema through aquaporin-4 downregulation. Exp Neurol 2011;227:89–95
22. McCoy E, Sontheimer H. Expression and function of water channels (aquaporins) in migrating malignant astrocytes. Glia 2007;55:1034–43
23. Manley GT, Fujimura M, Ma T, et al. Aquaporin-4 deletion in mice reduces brain edema after acute water intoxication and ischemic stroke. Nat Med 2000;6:159–63
24. Braak H, Braak E. Neuropathological stageing of Alzheimer-related changes. Acta Neuropathol 1991;82:239–59
25. Hoshi A, Nakahara T, Kayama H, et al. Ischemic tolerance in chemical preconditioning: Possible role of astrocytic glutamine synthetase buffering glutamate-mediated neurotoxicity. J Neurosci Res 2006;84:130–41
26. Sofroniew MV, Vinters HV. Astrocytes: Biology and pathology. Acta Neuropathol 2010;119:7–35
27. Allamann I, Bélanger M, Magistretti PJ. Astrocyte-neuron metabolic relationships: For better and for worse. Trends Neurosci 2011;34:76–87
28. Dorfman VB, Pasquini L, Riudavets M, et al. Differential cerebral deposition of IDE and NEP in sporadic and familial Alzheimer's disease. Neurobiol Aging 2010;31:1743–57
29. Verkman AS. More than just water channels: Unexpected cellular roles of aquaporins. J Cell Sci 2005;118:3225–32
30. Nuutinen T, Huuskonen J, Suuronen T, et al. Amyloid-β 1–42 induced endocytosis and clusterin/apoJ protein accumulation in cultured human astrocytes. Neurochem Int 2007;50:540–47
31. Rodríguez A, Pérez-Gracia E, Espinosa JC, et al. Increased expression of water channel aquaporin 1 and aquaporin 4 in Creutzfeldt-Jacob disease and in bovine spongiform encephalopathy-infected bovine-PrP transgenic mice. Acta Neuropathol 2006;112:573–85
32. Zhou S, Sun X, Liu L, et al. Increased expression of aquaporin-1 in the anterior temporal neocortex of patients with intractable epilepsy. Neurol Res 2008;30:400–5
33. Hayashi Y, Edwards N, Proescholdt MA, et al. Regulation and function of aquaporin-1 in glioma cells. Neoplasia 2007;9:777–87
34. Nesic O, Lee J, Unabia GC, et al. Aquaporin 1—A novel player in spinal cord injury. J Neurochem 2008;105:628–40
35. McCoy E, Sontheimer H. MAPK induces AQP1 expression in astrocytes following injury. Glia 2010;58:209–17
36. Satoh J, Tabunoki H, Yamamura T, et al. Human astrocytes express aquaporin-1 and aquaporin-4 in vitro and in vivo. Neuropathology 2007; 27:245–56
37. Fiala JC. Mechanism of amyloid plaque pathogenesis. Acta Neuropathol 2007;114:551–71
38. Attems J. Sporadic cerebral amyloid angiopathy: Pathology, clinical implications, and possible pathomechanisms. Acta Neuropathol 2005; 110:345–59
39. Richard E, Carrano A, Hoozemans JJ, et al. Characteristics of dyshoric capillary cerebral amyloid angiopathy. J Neuropathol Exp Neurol 2010; 69:1158–67
40. Wilcock DM, Vitek MP, Colton CA. Vascular amyloid alters astrocytic water and potassium channels in mouse models and humans with Alzheimer's disease. Neuroscience 2009;159:1055–69
41. Auguste KI, Jin S, Uchida K, et al. Greatly impaired migration of implanted aquaporin-4–deficient astroglial cells in mouse brain toward a site of injury. FASEB J 2007;21:108–16
42. Aoki-Yoshino K, Uchihara T, Duyckaerts C, et al. Enhanced expression of aquaporin 4 in human brain with inflammatory diseases. Acta Neuropathol 2005;110:281–88

Parkinsonism and Related Disorders 18 (2012) 677–679

Contents lists available at SciVerse ScienceDirect

Parkinsonism and Related Disorders

journal homepage: www.elsevier.com/locate/parkreldis

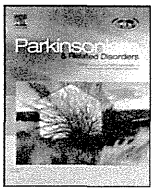

Letter to the Editor

A serial MRI study in a patient with progressive supranuclear palsy with cerebellar ataxia

Keywords:
Progressive supranuclear palsy
Cerebellar ataxia
Magnetic resonance imaging

Several clinical variants of progressive supranuclear palsy (PSP) have been identified [1]. We have recently defined a variant of patients designated PSP with cerebellar ataxia (PSP-C) [2]. Because these patients develop cerebellar ataxia as the initial and principal symptom, they might be clinically misdiagnosed as having spinocerebellar degeneration (SCD). To distinguish PSP-C from SCD, magnetic resonance imaging (MRI) [3] may be useful.

Here, we report the clinical course and serial MRI findings of a patient with pathologically proven PSP-C.

A 72-year-old Japanese man who developed unsteadiness of gait visited our hospital 1 year after its onset. Neurological examinations revealed supranuclear gaze palsy, axial rigidity, and limb and truncal ataxia. Although an initial brain MRI did not show obvious atrophy of the cerebellum (Fig. 1a–c), he was diagnosed as having SCD on the basis of clinical symptoms. Subsequently, the patient had frequent falls because of worsening of truncal ataxia. Two years after the onset, the second brain MRI was performed, which showed dilatation of pontocerebellar cistern (Fig. 1e,f) in addition to atrophy of the superior cerebellar peduncles (SCPs) (Fig. 1e). The third brain MRI, performed 4 years after the onset, showed the increased dilatation of pontocerebellar cistern, proportional but "small in size" pons and cerebellum with fourth ventricular dilatation (Fig. 1i), and the rostral midbrain atrophy (Fig. 1g). The progressive dilation of pontocerebellar cistern was confirmed by quantitative analyses: the area of pontocerebellar cistern at the level of middle cerebellar peduncles on the initial, second, and third MRIs are 7.5 mm^2 (12.6% of posterior fossa), 13.7 mm^2 (20.0% of posterior fossa), and 17.4 mm^2 (29.9% of posterior fossa), respectively (Fig. 1c,f,i). The progressive rostal midbrain atrophy was also confirmed [3]: the area of tegmentum mesencephali on the initial, second, and third MRIs are 103.8 mm^2, 69.2 mm^2, and 47.1 mm^2, respectively (Fig. 1a,d,g). At 76-year-old, he died from CO_2 narcosis. The diagnosis of PSP was confirmed after autopsy [2]. Briefly, tau-positive inclusion bodies in Purkinje cells (Fig. 2) and severe neuronal loss with gliosis in the dentate nucleus were observed.

We provide, for the first time, serial MRI findings in a pathologically proven PSP-C patient. When the patient developed cerebellar ataxia as an initial symptom, MRI did not show obvious atrophy of the cerebellum. However, follow-up MRI examinations demonstrated atrophy of the SCPs as well as dilatation of pontocerebellar cistern that accompanies "small in size" pons and cerebellum. The former finding has been shown on volumetric MR images in patients with PSP [3]. On the other hand, the latter finding was previously reported in a pathologically proven PSP patients who developed cerebellar ataxia as the initial and principal symptom: CT scans of the patient revealed no obvious atrophy of cerebellum in early-stage of the disease and enlarged pontocerebllar cistern in advanced-stage of the disease [4]. We consider that dilatation of pontocerebellar cistern that accompanies "small in size" pons and cerebellum might be characteristic imaging feature of PSP-C.

This patient is of interest to understand lesions responsible for ataxia in PSP patients. On the basis of our pathological examination of patients with PSP-C, we speculated that patients with tau-positive inclusion bodies in Purkinje cells and degenerated dentate nucleus easily develop cerebellar ataxia [2]. This speculation might be supported by a recent clinicopathological analysis of 30 Caucasian PSP patients, which demonstrated that cerebellar ataxia was exclusively observed in 2 patients who exhibited tau-positive inclusion bodies in Purkinje cells [5]. Future studies need to be performed to understand the mechanism by which cerebellum and pons become atrophic proportionally in PSP-C patients.

In conclusion, this case report suggest that dilatation of pontocerebellar cistern that accompanies "small in size" pons and cerebellum might be characteristic imaging feature of PSP-C, although accumulation of patients and analyses will be necessary.

1353-8020/$ – see front matter
doi:10.1016/j.parkreldis.2011.11.011

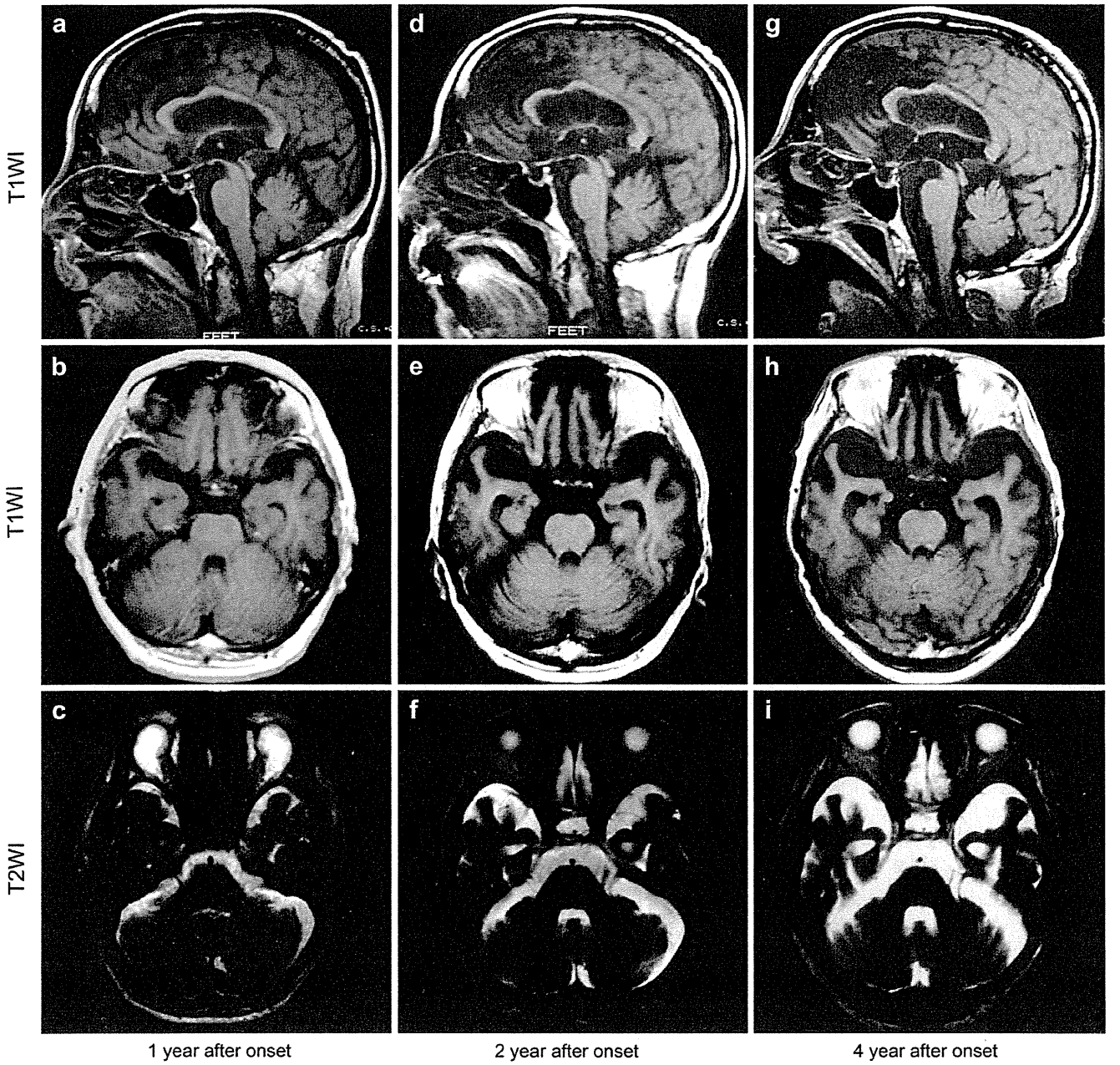

Fig. 1. A serial MRI study in the present patient. Top panels (a, d, g), sagittal T1-weighted MRIs (T1WIs) at the level of the mesencephalic aqueduct. Middle panels (b, e, h), axial T1WIs at the level of the superior cerebellar peduncles. Lower panels (c, f, i), axial T2-weighted MRIs (T2WIs) at the level of the middle cerebellar peduncles. Serial MRIs showed atrophies of the midbrain (g), superior cerebellar peduncles (e, h), and frontal and temporal lobes (e, h), in addition to enlarged pontocerebellar cistern without overt dilatation of cerebellar fissures (i).

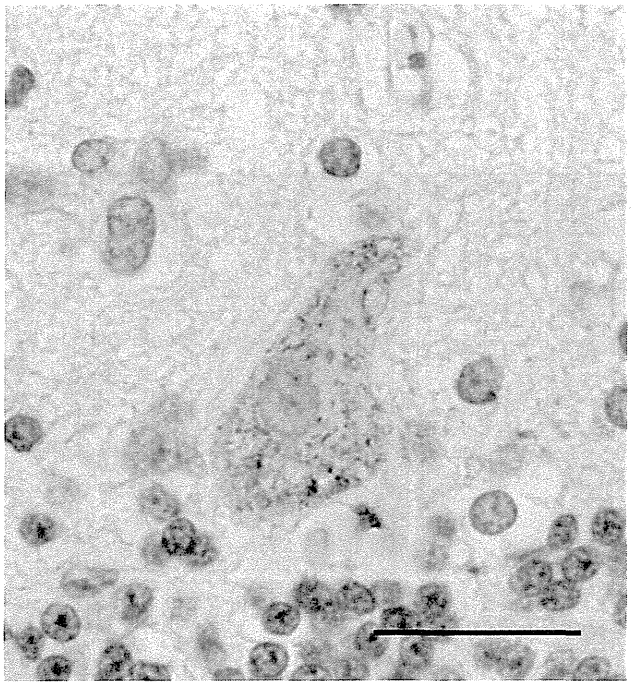

Fig. 2. Immunohistochemical finding of Purkinje cells. High-power magnifications view of a Purkinje cell demonstrating granular, tau-positive profiles in the cytoplasm by AT8 immunostain. Bar = 25 μm.

Disclosure

The authors report no conflicts of interest.

References

[1] Williams DR, Lees AJ. Progressive supranuclear palsy: clinicopathological concepts and diagnostic challenges. Lancet Neurol 2009;8:270–9.
[2] Kanazawa M, Shimohata T, Toyoshima Y, Tada M, Kakita A, Morita T, et al. Cerebellar involvement in progressive supranuclear palsy: a clinicopathological study. Mov Disord 2009;24:1312–8.
[3] Stamelou M, Knake S, Oertel WH, Hoglinger GU. Magnetic resonance imaging in progressive supranuclear palsy. J Neurol 2011;258:549–58.
[4] Aiba I, Saito Y, Yasuda T, Yoshida M, Hashizume Y. Progressive supranuclear palsy with cerebellar ataxia. An autopsy case. Shinkeinaika 2002;56:230–3 [in Japanese].
[5] Jellinger K. Cerebellar involvement in progressive supranuclear palsy. Mov Disord 2010;25:1104–5.

Masato Kanazawa, Takayoshi Shimohata*
Department of Neurology, Brain Research Institute, Niigata University, 1-757 Asahimachi-dori, Chuoku, Niigata, Niigata 951-8585, Japan

Kotaro Endo, Ryoko Koike
Department of Neurology, Nishi-Niigata Chuo National Hospital, Niigata, Japan

Hitoshi Takahashi
Department of Pathology, Brain Research Institute, Niigata University, Niigata, Japan

Masatoyo Nishizawa
Department of Neurology, Brain Research Institute, Niigata University, 1-757 Asahimachi-dori, Chuoku, Niigata, Niigata 951-8585, Japan

* Corresponding author. Tel.: +81 25 227 0666; fax: +81 25 223 6646.
E-mail address: t-shimo@bri.niigata-u.ac.jp (T. Shimohata)

30 September 2011

Human Molecular Genetics, 2013, Vol. 22, No. 15 **3003–3015**
doi:10.1093/hmg/ddt157
Advance Access published on April 4, 2013

Impaired viability of muscle precursor cells in muscular dystrophy with glycosylation defects and amelioration of its severe phenotype by limited gene expression

Motoi Kanagawa[1], Chih-Chieh Yu[1,†], Chiyomi Ito[1,†], So-ichiro Fukada[2], Masako Hozoji-Inada[1], Tomoko Chiyo[3], Atsushi Kuga[1], Megumi Matsuo[1], Kanoko Sato[1], Masahiko Yamaguchi[2], Takahito Ito[2], Yoshihisa Ohtsuka[1], Yuki Katanosaka[4], Yuko Miyagoe-Suzuki[3], Keiji Naruse[4], Kazuhiro Kobayashi[1], Takashi Okada[3], Shin'ichi Takeda[3] and Tatsushi Toda[1,*]

[1]Division of Neurology/Molecular Brain Science, Kobe University Graduate School of Medicine, Kobe 650-0017, Japan, [2]Laboratory of Molecular and Cellular Physiology, Graduate School of Pharmaceutical Sciences, Osaka University, Suita 565-0871, Japan, [3]Department of Molecular Therapy, National Institute of Neuroscience, National Center of Neurology and Psychiatry, Kodaira 187-8502, Japan and [4]Department of Cardiovascular Physiology, Graduate School of Medicine, Dentistry and Pharmaceutical Sciences, Okayama University, Okayama 700-8558, Japan

Received January 7, 2013; Revised March 3, 2013; Accepted April 2, 2013

A group of muscular dystrophies, dystroglycanopathy is caused by abnormalities in post-translational modifications of dystroglycan (DG). To understand better the pathophysiological roles of DG modification and to establish effective clinical treatment for dystroglycanopathy, we here generated two distinct conditional knock-out (cKO) mice for *fukutin*, the first dystroglycanopathy gene identified for Fukuyama congenital muscular dystrophy. The first dystroglycanopathy model—myofiber-selective fukutin-cKO [muscle creatine kinase (MCK)-fukutin-cKO] mice—showed mild muscular dystrophy. Forced exercise experiments in presymptomatic MCK-fukutin-cKO mice revealed that myofiber membrane fragility triggered disease manifestation. The second dystroglycanopathy model—muscle precursor cell (MPC)-selective cKO (Myf5-fukutin-cKO) mice—exhibited more severe phenotypes of muscular dystrophy. Using an isolated MPC culture system, we demonstrated, for the first time, that defects in the fukutin-dependent modification of DG lead to impairment of MPC proliferation, differentiation and muscle regeneration. These results suggest that impaired MPC viability contributes to the pathology of dystroglycanopathy. Since our data suggested that frequent cycles of myofiber degeneration/regeneration accelerate substantial and/or functional loss of MPC, we expected that protection from disease-triggering myofiber degeneration provides therapeutic effects even in mouse models with MPC defects; therefore, we restored fukutin expression in myofibers. Adeno-associated virus (AAV)-mediated rescue of fukutin expression that was limited in myofibers successfully ameliorated the severe pathology even after disease progression. In addition, compared with other gene therapy studies, considerably low AAV titers were associated with therapeutic effects. Together, our findings indicated that fukutin-deficient dystroglycanopathy is a regeneration-defective disorder, and gene therapy is a feasible treatment for the wide range of dystroglycanopathy even after disease progression.

*To whom correspondence should be addressed at: 7-5-1 Kusunoki-chou Chuo-ku, Kobe 650-0017, Japan. Tel: +81 783826287; Fax: +81 783826288; Email: toda@med.kobe-u.ac.jp
†These authors contributed equally to this work.

INTRODUCTION

Dystroglycanopathy includes Walker–Warburg syndrome, muscle–eye–brain disease, Fukuyama congenital muscular dystrophy (FCMD) and several forms of congenital and limb–girdle muscular dystrophies (1). Dystroglycanopathy is indicated by a wide variety of clinical symptoms; the most severe end of the clinical spectrum is characterized by congenital muscular dystrophy with severe structural brain and eye abnormalities, whereas the mildest end presents in adult life with limb–girdle muscular dystrophy without brain or eye involvement (1). FCMD is the first dystroglycanopathy to be reported (2,3), and it is the second most common childhood muscular dystrophy in Japan. The founder mutation, a SINE-VNTR-*Alu* retrotransposon insertion in the 3′ noncoding region of *fukutin*, causes abnormal splicing that leads to the production of non-functional proteins in FCMD (4,5). FCMD is characterized by severe congenital muscular dystrophy, abnormal neuronal migration associated with mental retardation and epilepsy and, frequently, eye abnormalities. It often results in early death before the age of 20 (6). Several point mutations in *fukutin* have also been reported to be associated with dystroglycanopathy in Japan and other countries (7,8).

More than 10 genes [protein *O*-mannosyltransferase 1 (*POMT1*), protein *O*-mannosyltransferase 2 (*POMT2*), protein *O*-linked mannose β-1,2-*N*-acetylglucosaminyltransferase 1 (*POMGNT1*), *fukutin*, fukutin-related protein (*FKRP*), *LARGE*, dolichol-phosphate-mannose synthase (*DPM2* and *DPM3*), isoprenoid synthase domain containing (*ISPD*) gene, glycosyltransferase-like domain containing 2 (*GTDC2*) gene and β-1,3-*N*-acetylglucosaminyltransferase 1 (*B3GNT1*)], implicated in dystroglycanopathies, have been shown or expected to be involved in the glycosylation pathway of α-dystroglycan (α-DG) (1,9,10). POMGnT1 and the POMT1/2 complex possess glycosyltransferase activities and can directly synthesize *O*-mannosyl sugar chains on α-DG (11,12). Fukutin, FKRP and LARGE are involved in a novel phosphodiester-linked modification, namely, a post-phosphoryl modification, of *O*-mannose on α-DG (13,14). Recently, it has been shown that LARGE can act as a bifunctional glycosyltransferase with both xylosyltransferase and glucuronyltransferase activities (15). The DG gene *DAG1* encodes both α- and β-DG, which is post-translationally cleaved into the two subunits (16). α-DG is a highly glycosylated protein and serves as the receptor subunit for extracellular proteins such as laminins, perlecan, agrin, neurexin and pikachurin (9,17). *O*-mannosyl glycosylation and the post-phosphoryl modification are required for the ligand-binding activities of α-DG (3,13). Hypoglycosylation and reduced ligand-binding activity of α-DG are common characteristics of dystroglycanopathy. α-DG is anchored to the plasma membrane through non-covalent interactions with the transmembrane subunit β-DG. β-DG intracellularly interacts with dystrophin, whose mutations lead to Duchenne/Becker muscular dystrophy, and dystrophin, in turn, binds to actin filaments. This molecular linkage, created by laminin-DG-dystrophin-actin filaments, is thought to provide mechanical stability to the plasma membrane of the muscle fiber; thus, disruption of this linkage is considered a key pathological event in several forms of muscular dystrophy. In FCMD skeletal muscles, in addition to dystrophic muscular changes, there are certain characteristics such as intensive connective tissue infiltration and the presence of predominant small-sized fibers from the early infantile stage (6). Furthermore, aberrant neuromuscular junctions and delayed muscle fiber maturation have been implicated in the pathology of FCMD (18). FCMD also shows central nervous system involvement. Together, these data suggest that more complex and unknown physiological roles of α-DG modification underlie the skeletal muscle pathology of dystroglycanopathy.

Recent studies have identified new genes associated with dystroglycanopathy (19–21), and an increasing number of patients are being diagnosed with dystroglycanopathy worldwide. However, the pathogenesis of this condition is not fully understood, and no effective clinical treatment has been established. To understand the pathogenesis and establish a therapeutic strategy for dystroglycanopathy, we developed two distinct *fukutin* conditional knock-out (cKO) mice as models for dystroglycanopathy. In our study, investigation of presymptomatic fukutin-deficient mice provided direct evidence that fragility of the myofiber membrane triggers the pathogenesis of dystroglycanopathy. We also used an isolated muscle precursor cell (MPC) culture system to demonstrate, for the first time, that defects in the fukutin-dependent modification of DG lead to impairment of MPC proliferation, differentiation and muscle regeneration. We predicted that protection from disease-triggering myofiber degeneration would prevent substantial and/or functional loss of MPC, thereby providing therapeutic effects. Indeed, we demonstrate that restoration of fukutin expression in myofibers successfully ameliorates the severe pathology even after disease progression. These results indicate that gene therapy is a feasible treatment for dystroglycanopathy.

RESULTS

Generation and characterization of myofiber-selective fukutin cKO mice

To generate *fukutin*-cKO mice, flox fukutin mice (*fukutin*$^{lox/lox}$) were crossed with muscle creatine kinase (MCK)-Cre mice (22) or Myf5-Cre mice (23), which express the *Cre* gene with the help of the MCK promoter or Myf5 promoter, respectively (Supplementary Material, Fig. S1). The MCK promoter is active in differentiating and differentiated muscle cells (24), and MCK expression reaches maximum levels at post-natal day 10 and remains constantly high throughout life (25). First, we analyzed the MCK-fukutin-cKO mice at different time points. In the skeletal muscles of these mice, we confirmed dramatic reduction in the fukutin protein after the age of 4 weeks (Fig. 1A). Abnormal modification of α-DG is indicated by decreased molecular weight, loss of immunoreactivity against the monoclonal IIH6 antibody, which recognizes properly glycosylated α-DG (3), and decreased laminin-binding activity. Abnormally modified α-DG was predominant in MCK-fukutin-cKO mice aged >8 weeks (Fig. 1A). Loss of the post-phosphoryl modification was further confirmed by subjecting the protein to treatment with cold aqueous hydrofluoric (HF) acid, which cleaves phosphoester linkages, and to inorganic metal-affinity chromatography (IMAC), which captures monoester-linked phosphorylated compounds

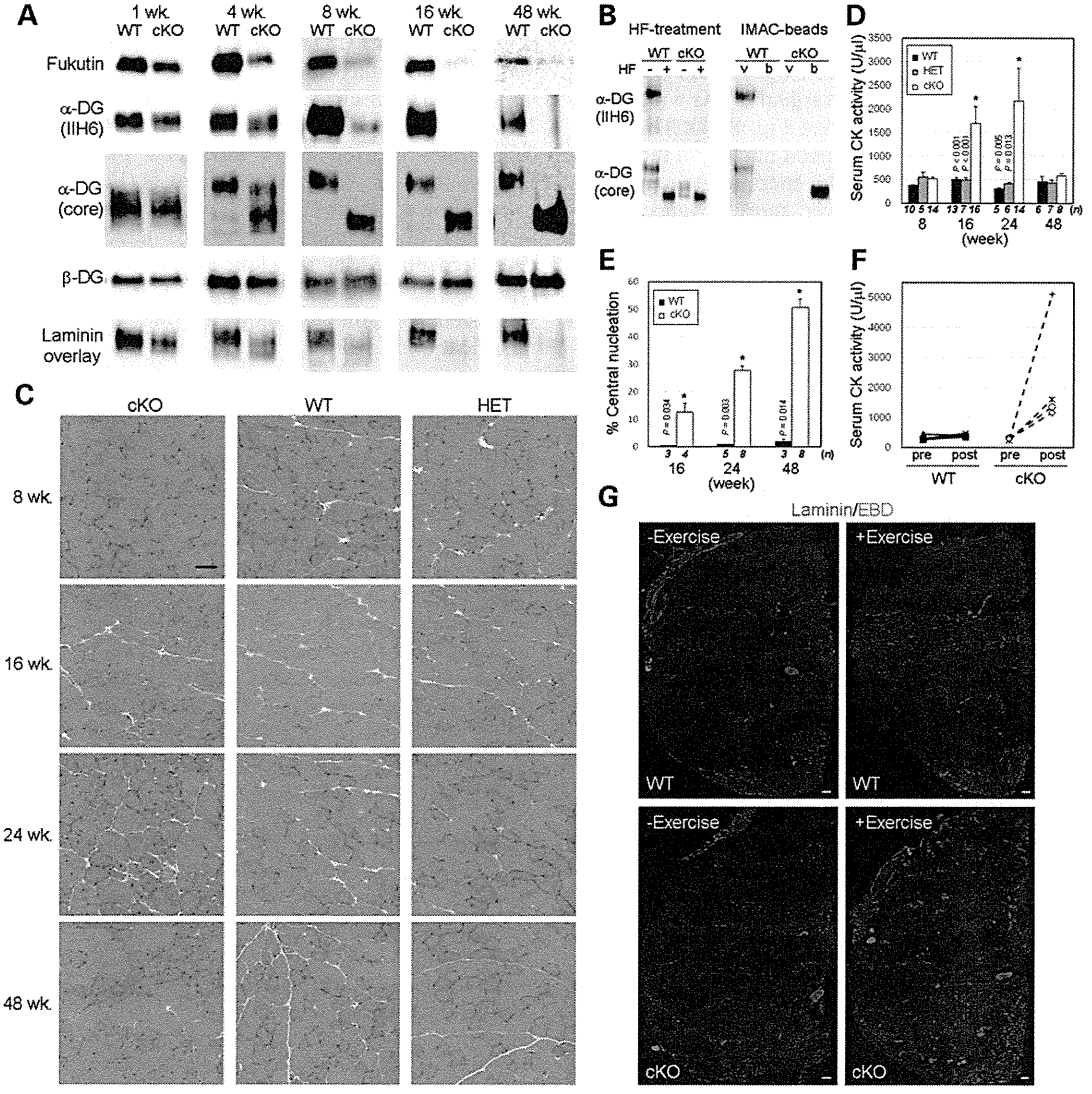

Figure 1. Pathological characterization of MCK-fukutin-cKO mice. (**A**) Western blot analysis of fukutin protein expression and α-DG modification in MCK-fukutin-cKO (cKO) and litter control WT skeletal muscles at different ages (1, 4, 8, 16 and 48 weeks). β-DG was used as a loading control. Laminin-binding activity of α-DG was examined by the laminin overlay assay. (**B**) Post-phosphoryl modification of α-DG from MCK-fukutin-cKO and control WT skeletal muscles. The absence of the post-phosphoryl modification was confirmed by HF treatment and IMAC-bead-binding assay. The void (v) and bound (b) fractions of the IMAC beads were analyzed by western blotting. (**C**) H&E staining of tibialis anterior muscles. Bar = 50 μm. (**D**) Serum CK activity and (**E**) proportion of myofibers with centrally located nuclei. Data shown are mean ± SEM for each group (*n* is indicated in the graph). $^*P \leq 0.05$ for both cKO versus WT and cKO versus HET (D) and cKO versus WT (E) (Mann–Whitney *U* test; *P*-values are indicated in the graph). (**F**) Serum CK activity before and after forced exercise. Serum CK levels of individual mice ($n = 4$ in each genotype) were measured before (pre) and after (post) exercise. (**G**) Uptake of Evans blue dye into myofibers after forced exercise. MCK-fukutin-cKO and control WT mice were subjected to forced exercise (+Exercise); subsequently, the muscle sections were stained with laminin (green) for individual fibers and merged with Evans blue dye (red). Mice not subjected to exercise were used as controls (−Exercise). Bar = 200 μm.

(13,14). The molecular weight of α-DG in the skeletal muscles of control (WT) mice was dramatically reduced after HF treatment, and α-DG did not bind to IMAC beads because the phosphodiester-linked modification was intact; in contrast, α-DG in the skeletal muscles of MCK-fukutin-cKO mice showed little sensitivity to HF and bound to IMAC beads (Fig. 1B), indicating incomplete post-phosphoryl modification. Immunofluorescence staining with an antibody against an α-DG core protein showed that α-DG localized to the sarcolemma of MCK-fukutin-cKO mice as seen in normal controls (Supplementary Material, Fig. S2A), which suggests that cellular trafficking of α-DG is little affected by fukutin deficiency. These results confirmed abnormal modification of α-DG in the skeletal muscles of MCK-fukutin-cKO mice.

Hematoxylin and eosin (H&E) staining revealed that 16-week-old MCK-fukutin-cKO mice showed signs of muscular dystrophy, such as myonecrosis and central nucleation (Fig. 1C). Serum creatine kinase (CK) activity in

16-week-old MCK-fukutin-cKO mice was significantly higher than that in controls (Fig. 1D). These pathological features were not observed in 8-week-old mice (Fig. 1C and D); a possible reason may be the presence of residual α-DG with proper glycosylation (Supplementary Material, Fig. S2B). The population of myofibers with centrally located nuclei, an indication of repeated cycles of myofiber degeneration/regeneration, increased with age (Fig. 1E); however, more advanced pathology, such as infiltration of fat and connective tissues, was rarely observed even in 48-week-old MCK-fukutin-cKO mice (Fig. 1C).

It has been widely believed that functional and/or substantial loss of DG-containing protein complexes (i.e. the dystrophin–glycoprotein complex) leads to disease-causing membrane fragility. This concept is based on results of forced exercise experiments in animals with muscular dystrophy, which led to increases in the serum CK levels and uptake of membrane-impermeable Evans blue dye by myofibers (26,27). However, these experiments were conducted in diseased animals; therefore, it remains unclear whether membrane fragility triggers disease-causing phenotype. Therefore, we subjected 10-week-old MCK-fukutin-cKO mice, which showed abnormal α-DG modification but no pathology (Supplementary Material, Fig. S2C), to forced exercise. After forced exercise, serum CK levels were dramatically increased in the MCK-fukutin-cKO mice but not in the control mice (Fig. 1F). Myofibers with membrane-impermeable Evans blue dye uptake were also observed only in the exercise-administered MCK-fukutin-cKO mice (Fig. 1G). These data indicate that the plasma membrane of the muscle cells becomes weak before disease onset, providing proof-of-principle that membrane fragility triggers disease manifestation.

Characterization of MPC-selective fukutin cKO mice

Loss of fukutin in differentiated myofibers results in only mild and slow-progressing disease-causing phenotypes. We hypothesized that fukutin-dependent modification also plays a role in MPCs that are not targeted by MCK-Cre-mediated recombination. Therefore, we generated cKO mice lacking fukutin in MPCs by crossing flox fukutin mice with Myf5-Cre knock-in mice (23) expressing Cre recombinase under the control of the endogenous Myf5 promoter (Myf5-fukutin-cKO mice; Supplementary Material, Fig. S1). It has been reported that the Myf5-Cre allele recapitulates the expression pattern of the endogenous Myf5 gene and is uniformly expressed in all proliferating myoblasts (23). The Myf5-fukutin-cKO mice grossly show little difference compared with the litter controls until ~2 weeks of age; thereafter, increase in body weight was significantly retarded (Fig. 2A). Most Myf5-fukutin-cKO mice died by 6 months (Fig. 2B). Reduction in fukutin protein expression and abnormal modification were confirmed by immunofluorescence, western blotting, HF treatment and IMAC-bead assay (Fig. 2C and D). As is the case of MCK-fukutin-cKO, α-DG in Myf5-fukutin-cKO localizes to the sarcolemma (Supplementary Material, Fig. S2D). H&E staining revealed progressive pathological changes in Myf5-fukutin-cKO skeletal muscles (Fig. 2E). At 2 weeks, myonecrotic fibers were sparse (Supplementary Material, Fig. S2E), and at 4 weeks, in addition to myonecrotic fibers, myofibers with centrally located nuclei were observed (Fig. 2E). Serum CK levels and the proportion of the myofibers with centrally located nuclei were significantly higher in Myf5-fukutin-cKO mice than in the controls at 4, 8 and 16 weeks (Fig. 2F and G). Sixteen-week-old Myf5-fukutin-cKO mice showed more advanced pathological changes, such as fiber size variation and fibrosis (Fig. 2E). A few specimens showed milder phenotypic changes accompanied by increases in the normally glycosylated α-DG population (Supplementary Material, Fig. S2F). Overall, different phenotypes of the MCK-fukutin-cKO and Myf5-fukutin-cKO mice suggested a pathophysiological role of fukutin-dependent modification in MPCs.

Impaired viability of MPCs in Myf5-fukutin-cKO mice

To determine the impact of fukutin deficiency on MPC activity, we isolated SM/C-2.6(+) satellite cells from young (slightly affected) and adult (diseased) Myf5-fukutin-cKO muscles and then cultured them as MPCs (i.e. myoblasts) (28). The number of isolated SM/C-2.6(+) cells tended to be less in young fukutin-deficient muscles and was significantly reduced in adults compared with the litter controls (Fig. 3A). The proliferation activity of the isolated MPCs was slightly but significantly decreased in young and severely reduced in adult Myf5-fukutin-cKO muscles (Fig. 3B). The differentiation activity of fukutin-deficient myoblasts was significantly lower than that of the control mice (Fig. 3C). Quantification of the Pax7 immunofluorescence signal, a satellite cell marker, on skeletal muscle sections also suggested decreases in the number of satellite cells in adult Myf5-fukutin-cKO mice compared with control mice (Supplementary Material, Fig. S3A). We also examined the population of activated satellite cells by Pax7/MyoD double staining on the skeletal muscle sections from Myf5-fukutin-cKO mice. The results suggested that the number of active satellite cells was reduced in 16-week-old Myf5-fukutin-cKO mice compared with that in 8-week-old Myf5-fukutin-cKO mice (Supplementary Material, Fig. S3B). These data suggest that in addition to decreases in the number of satellite cells, the activation state of satellite cells is impaired in Myf5-cKO mice as the disease progresses.

We next examined *in vivo* regeneration capability of the Myf5-fuktuin-cKO muscles after cardiotoxin (CTX)-induced muscle degeneration. After 14 days of the CTX challenge in adult mice (~3 months old), we observed that the proportion of small myofibers was strikingly higher in Myf5-fukutin-cKO mice than in the controls (Fig. 3D and E). In some cases, the CTX-injected Myf5-fukutin-cKO muscles showed severe atrophic changes compared with the contralateral saline-injected ones (Supplementary Material, Fig. S3C). In younger (~4 weeks old) Myf5-fukutin-cKO mice, after 14 days of the CTX challenge, no obvious histological difference was noted compared with the controls (Supplementary Material, Fig. S3D); however, after 5 days of the CTX challenge, the proportion of smaller regenerating fibers (that are embryonic myosin-positive) was higher in Myf5-fukutin-cKO muscles than in the controls (Supplementary Material, Fig. S3E and F). These minor impairments in the regeneration of younger Myf5-fukutin-cKO skeletal muscles are consistent with the *in vitro* results. Overall, our data showed that fukutin-dependent

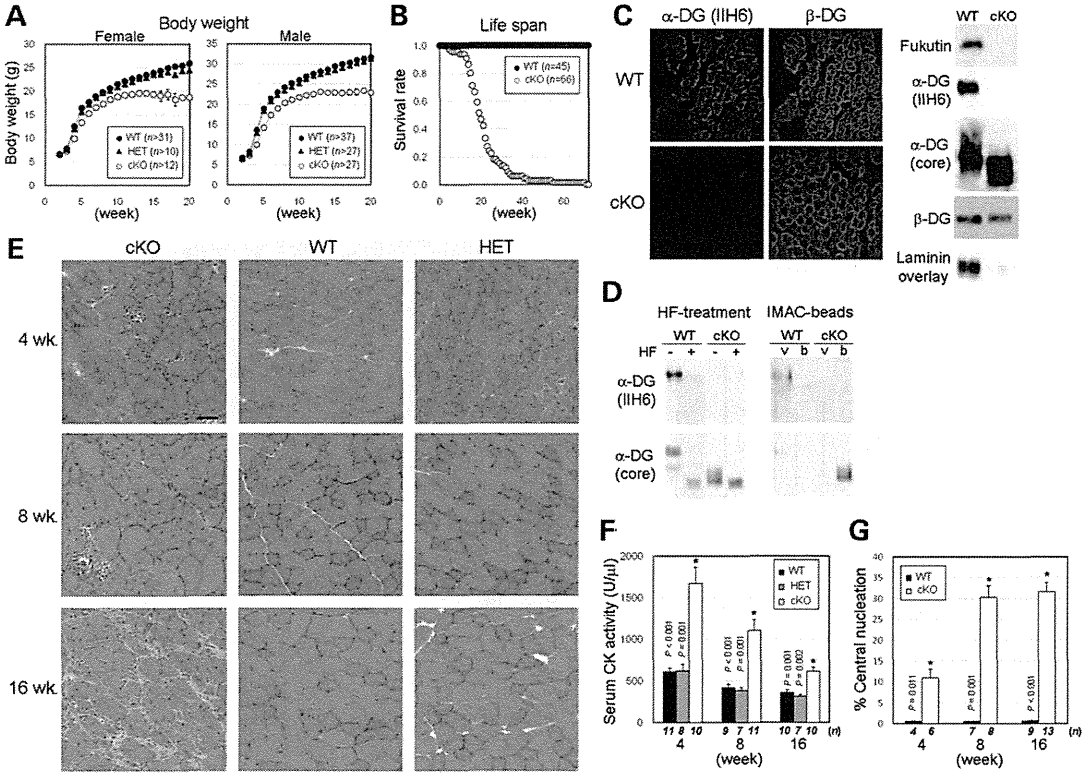

Figure 2. Pathological characterization of Myf5-fukutin-cKO mice. (**A**) Temporal changes in body weight. Data shown are mean ± SEM for each group (*n* is indicated in the graph). (**B**) Survival curve of Myf5-fukutin cKO mice. (**C**) Immunofluorescence and western blot analyses of fukutin expression and α-DG modification. Skeletal muscles of new born and 1-week-old Myf5-fukutin-cKO and control WT mice were used for immunofluorescence and western blotting, respectively. β-DG was used as a control. Laminin-binding activity of α-DG was examined by the laminin overlay assay. (**D**) Post-phosphoryl modification of α-DG from Myf5-fukutin-cKO and control WT skeletal muscles. The absence of post-phosphoryl modification was tested by HF treatment and IMAC-bead-binding assay. The void (v) and bound (b) fractions of the IMAC beads were analyzed by western blotting. (**E**) H&E staining of tibialis anterior muscles. Bar = 50 μm. (**F**) Serum creatin kinase activity and (**G**) proportion of myofibers with centrally located nuclei. Data shown are mean ± SEM for each group (*n* is indicated in the graph). $^*P \leq 0.05$ for both cKO versus WT and cKO versus HET (F) and cKO versus WT (G) (Mann–Whitney *U* test; *P*-values are indicated in the graph).

modification plays important roles in maintaining MPC viability, and consequently, muscle regeneration capability, suggesting that these defects may contribute to the severe phenotype of dystroglycanopathy.

Amelioration of the severe pathology by limited fukutin rescue in myofibers

Our pathological analysis of the two distinct fukutin-cKO mice suggested that membrane fragility triggers disease manifestation and that impaired MPC viability is related to disease progression and severity of dystroglycanopathy. These findings indicate that a therapeutic strategy must involve prevention of myofiber membrane weakness and/or rescue of substantial loss and dysfunction of MPCs. In addition, dystroglycanopathy is usually diagnosed after disease manifestation, and thus, treatments should be effective even after disease progression. Since our data suggested that frequent cycles of myofiber degeneration/regeneration accelerate substantial and/or functional loss of MPC, we expected that protection from disease-triggering myofiber degeneration provides therapeutic effects even in mouse models with MPC defects. In this study, to prevent disease-causing myofiber degeneration, we examined whether rescue of fukutin expression that is limited in myofibers is therapeutically beneficial in Myf5-fukutin-cKO mice. Therefore, we constructed recombinant AAV9 (AAV, adeno-associated virus) vectors containing the mouse *fukutin* cDNA under the MCK promoter (AAV9-MCK-*fukutin*).

We first administered intramuscular injections of AAV9-MCK-*fukutin* to 1-week-old (i.e. before disease manifestation) or 8-week-old (i.e. after disease manifestation) Myf5-fukutin-cKO mice; then, we examined the therapeutic effects after 2 months. In both cases, fukutin protein expression was higher in the AAV-injected Myf5-fukutin-cKO muscles than in the control WT muscles (endogenous fukutin protein in muscle lysates is below detectable levels) (Fig. 4A and E). IIH6-positive α-DG was restored, indicating functional rescue of *fukutin* gene expression even in adult cases (Fig. 4A, B, E and F). Histological and quantitative analyses showed that gene transfer at 1 week prevented disease manifestation (Fig. 4C and D). When gene transfer was challenged in 8-week-old mice, H&E staining showed milder phenotype in AAV-treated Myf5-fukutin-cKO muscles than

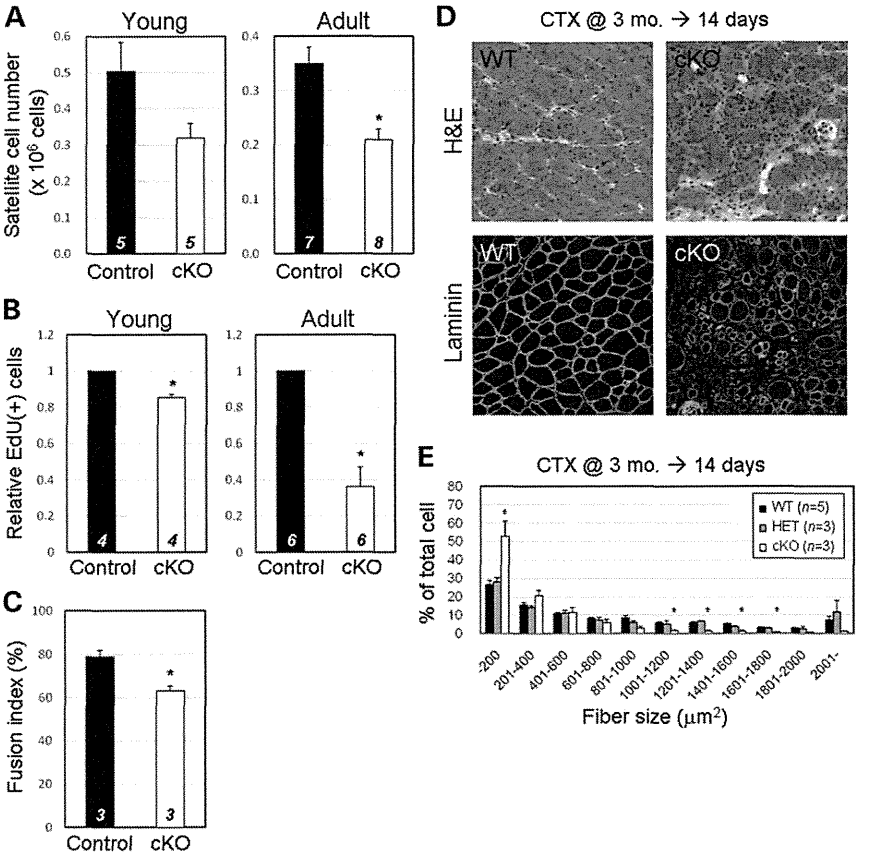

Figure 3. Impaired MPC activities and muscle regeneration in Myf5-fukutin-cKO mice. (**A**) The number of isolated satellite cells from young (2 weeks old) and adult (4 months old) Myf5-fukutin-cKO mice. $P = 0.117$ for young, and $P = 0.005$ for adult (Mann–Whitney U test). (**B**) Proliferation activity of the isolated MPCs. MPCs from young or adult Myf5-fukutin-cKO muscles were cultured for 2 days, and 5-ethynyl-2′-deoxyuridine-positive (EdU+) cells were counted. $P = 0.014$ for young, and $P = 0.002$ for adult (Mann–Whitney U test). (**C**) Differentiation activity of the isolated MPCs. MPCs from young Myf5-fukutin-cKO muscles were cultured in growth media for 2 days and then in differentiation media for 2 days. The cells were fixed, and multinucleated myotubes were counted. $P = 0.05$ (Mann–Whitney U test). For (A)–(C), data shown are mean ± SEM for each group (n is indicated in the graph). $^*P \leq 0.05$ compared with litter controls (Mann–Whitney U test). (**D**) Regeneration after CTX-induced muscle degeneration. CTX was injected into the tibialis anterior muscles of 3-month-old Myf5-fukutin-cKO and control mice (WT and HET). After 14 days, the muscle sections were analyzed by H&E staining and immunofluorescence staining with laminin. (**E**) Quantitative analysis for myofiber size variation after the CTX challenge. Data shown are mean ± SEM for each group (n is indicated in the graph). $^*P \leq 0.05$ for both cKO versus WT and cKO versus HET (Mann–Whitney U test).

in non-treated ones (Fig. 4G). Quantitatively, connective tissue infiltration and prevalence of small fibers were significantly reduced (Fig. 4H and I), whereas a substantial number of myofibers with central nucleation was still present after the gene transfer (Fig. 4J).

Next, we examined systemic delivery of the *fukutin* gene via tail vein injection into 4-week-old Myf5-fukutin-cKO mice with early-stage muscular dystrophy, primarily because diagnosis occurs during this stage in humans. After 2 months of the injection, we confirmed fukutin protein expression and recovery of α-DG modification in the treated Myf5-fukutin-cKO mice (Fig. 5A and B). After gene transfer, body and muscle weight were restored (Fig. 5C and D), and grip strength was dramatically improved, indicating recovery of muscle physiological function (Fig. 5E). H&E staining (Fig. 5F) and quantitative analyses of connective tissue infiltration (Fig. 5G) and fiber size variation (Fig. 5H) showed amelioration of muscle pathology; however, there were still a few necrotic fibers and a substantial proportion of myofibers with centrally located nuclei (Fig. 5I). Similar therapeutic effects were also obtained in other muscles (Supplementary Material, Fig. S4). Our results show that limited recovery of fukutin expression in myofibers, even after disease progression, can successfully ameliorate the severe phenotype of Myf5-fukutin-cKO mice.

We also constructed recombinant AAV9 vectors containing the mouse *fukutin* cDNA under the CMV promoter (AAV9-CMV-*fukutin*), which is commonly used for driving the expression of transgenes in a wide range of cell types. Two months after tail-vein injection in 4-week-old Myf5-fukutin-cKO mice, we observed therapeutic effects similar to those observed in AAV9-MCK-*fukutin*-treated Myf5-fukutin-cKO mice (Supplementary Material, Fig. S5). There was no obvious difference in the efficiency for the recovery of IIH6 immunoreactivity (the proportion of IIH6-positive to laminin-positive fibers) between the cases of AAV9-MCK-*fukutin* (77.4 ± 3.8%, $n = 5$) and AAV9-CMV-*fukutin* (74.8 ± 3.6%,

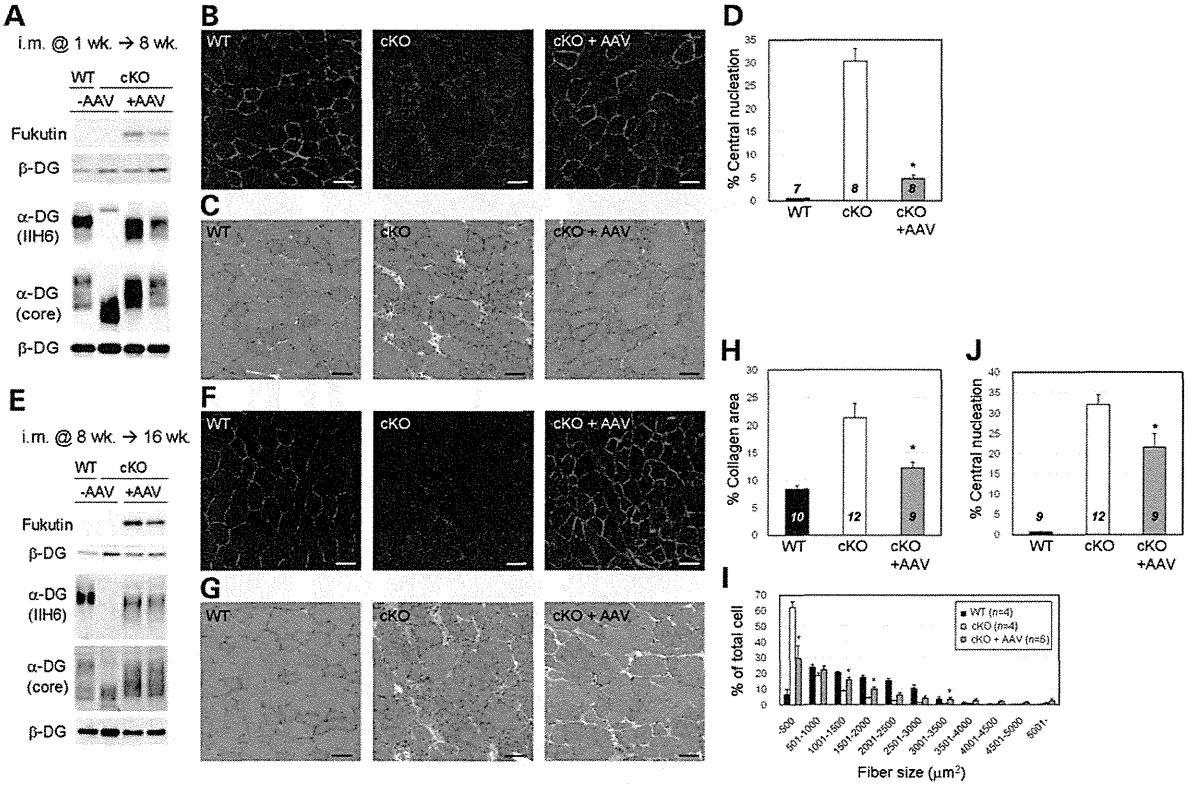

Figure 4. Gene transfer of *fukutin* via AAV9 intramuscular injection into Myf5-fukutin-cKO mice. AAV9-MCK-*fukutin* was administered to 1-week-old (**A**–**D**) and 8-week-old (**E**–**J**) Myf5-fukutin-cKO mice via intramuscular injection. Two months after the gene transfer, recovery of fukutin protein and α-DG glycosylation was confirmed by western blotting (A and E) and IIH6-immunofluorescence staining (B and F) (bar = 50 μm). For fukutin protein expression and α-DG modification, total lysate and wheat germ agglutinin-enriched fractions, respectively, were subjected to western blotting. In both cases, β-DG was used as a loading control. Western blotting results for two AAV-treated mice are shown. Therapeutic effects were quantitatively evaluated in terms of the proportion of myofibers with centrally located nuclei (D; $P = 0.001$, J; $P = 0.023$), connective tissue infiltration (H; $P = 0.016$) and fiber size variation (I; $^*P \leq 0.05$). Data shown are mean ± SEM for each group (n is indicated in the graph). $^*P \leq 0.05$ compared with non-treated cKO mice (Mann–Whitney U test).

$n = 5$). In addition, the population of myofibers with centrally located nuclei was significantly improved (Supplementary Material, Fig. S5I). We also examined the effects of intraperitoneal injections of AAV9-CMV-*fukutin* in 1-week-old Myf5-fukutin-cKO mice. Two months after the injections, we observed partial recovery of α-DG glycosylation and amelioration of the pathology compared with that observed in non-treated Myf5-fukutin-cKO mice (Supplementary Material, Fig. S6A–D).

The predominant mutation in FCMD is a retrotransposon insertion (4). We previously generated a transgenic knock-in mouse model carrying this insertion (29). The knock-in Hp/− mice represent compound heterozygotes for the insertion and a nonsense *fukutin* mutation. Although Hp/− mice show abnormal glycosylation of α-DG, a small amount of intact α-DG is also present; this prevents muscular dystrophy (29). We administered intraperitoneal injections of AAV9-CMV-*fukutin* to 1-week-old Hp/− mice and examined α-DG glycosylation status after 16 and 48 weeks. We detected increased levels of fukutin expression and IIH6-positive α-DG in the AAV-treated Hp/− skeletal muscles even 48 weeks after the gene transfer (Supplementary Material, Fig. S6E). These data suggest that the transferred *fukutin* gene persists in correcting abnormal glycosylation of α-DG for a considerable length of time.

DISCUSSION

In this study, we developed and analyzed two distinct *fukutin* cKO mice to understand the pathogenesis and to establish a therapeutic strategy for dystroglycanopathy. Our data showed that MPC-selective Myf5-fukutin-cKO mice exhibited more severe phenotypes of muscular dystrophy than myofiber-selective MCK-fukutin-cKO mice. Very recently, Campbell and colleagues also generated *fukutin* cKO mice, using Myf5-Cre and MCK-Cre mice (30). Pathological analysis of our Myf5-fukutin-cKO and MCK-fukutin-cKO mice showed results that were mostly consistent with those reported by Campbell and colleagues: increased serum CK levels in both cKO lines; milder phenotypes of MCK-fukutin-cKO than Myf5-fukutin-cKO; and decreases in grip strength, body mass and longevity of Myf5-fukutin-cKO mice. Our study includes further detailed histopathological characterization of the disease onset and progression in both lines. More importantly, our present study clarifies features of dystroglycanopathy that

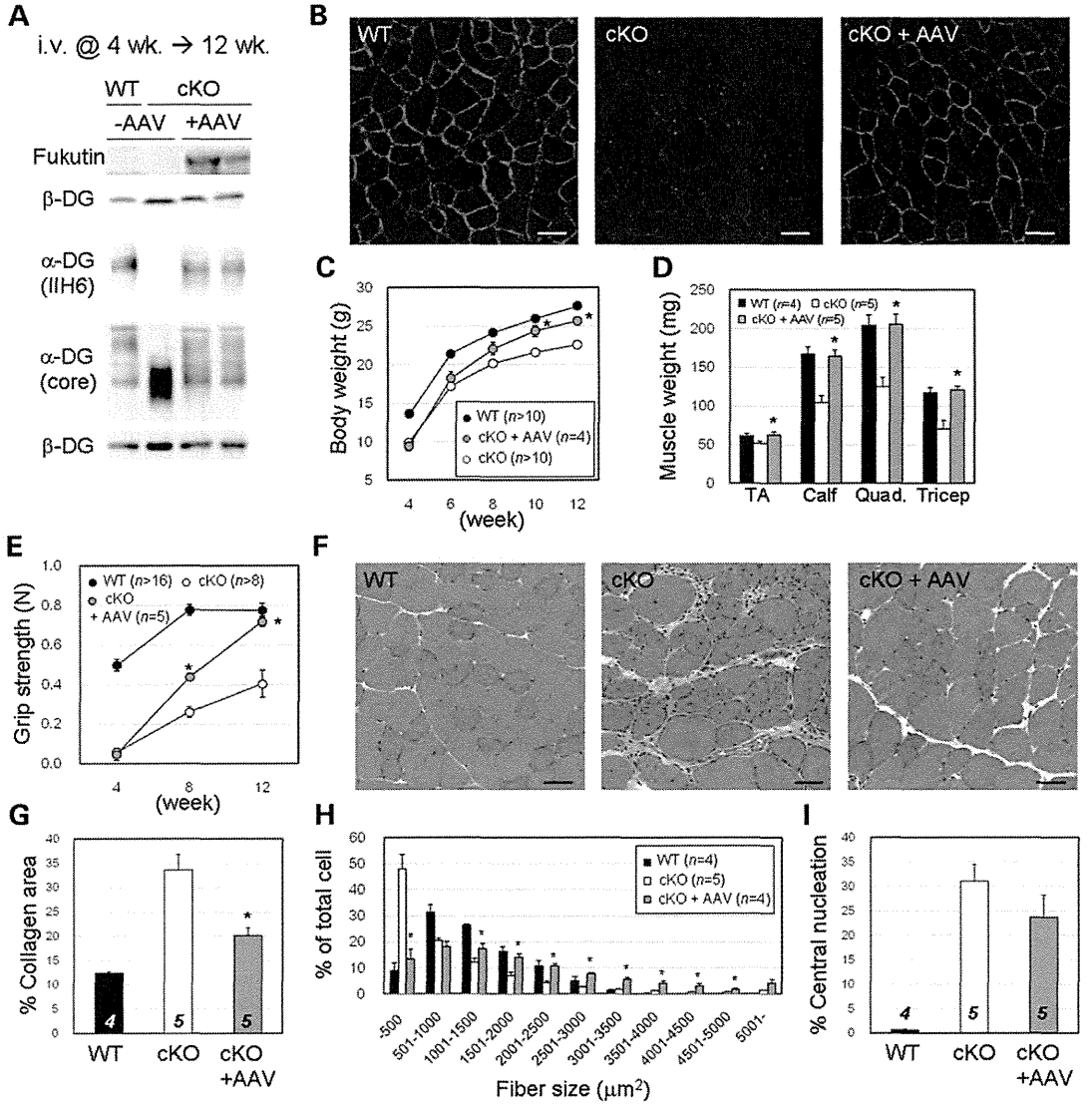

Figure 5. Systemic gene transfer of *fukutin* into Myf5-fukutin-cKO mice. AAV9-MCK-*fukutin* was administered to 4-week-old Myf5-fukutin-cKO mice via tail vein injection. Two months after the gene transfer, the skeletal muscles were analyzed and compared with non-treated Myf5-fukutin-cKO muscles. Recovery of fukutin protein and α-DG modification was confirmed by western blotting (**A**) and immunofluorescence (**B**) (bar = 50 μm). For fukutin protein expression and α-DG modification, total lysate and wheat germ agglutinin-enriched fractions, respectively, were subjected to western blotting. In both cases, β-DG was used as a loading control. Therapeutic effects were evaluated by body weight change (**C**; $P = 0.016$ and 0.01 for 10 and 12 weeks, respectively) and muscle weight change (**D**; $P = 0.047$ for tibialis anterior, and 0.014 for other muscles), grip strength (**E**; $P = 0.007$ and 0.003 for 8 and 12 weeks, respectively), H&E staining (**F**) (bar = 50 μm), connective tissue infiltration estimated by quantification of collagen I immunoreactive areas (**G**; $P = 0.028$), fiber size variation (**H**; $^*P \leq 0.05$) and central nucleation (**I**). Data from the tibialis anterior muscle are shown (F–I). Histopathology (F) and quantitative analyses (G and H) indicate amelioration of disease severity after the gene transfer. Data shown are mean ± SEM for each group (*n* is indicated in the graph). $^*P \leq 0.05$ compared with the non-treated cKO mice (Mann–Whitney *U* test). TA, tibialis anterior; Quad., quadricep.

enhance our understanding of its pathogenesis—specifically, the trigger initiating disease pathogenesis and the biological mechanism underlying the severe phenotype.

Our study provides direct evidence using presymptomatic fukutin-deficient mice that myofiber membrane fragility triggers disease manifestation. Although histological data in both studies suggested regeneration delay or impairment in Myf5-fukutin-cKO skeletal muscles, our study provides the first direct evidence for impaired MPC activity and viability using the isolated myoblast culture system. We observed that the proliferation and differentiation activities of the isolated MPCs from little-affected young Myf5-fukutin-cKO muscles were decreased, which may suggest that fukutin-dependent modification of α-DG plays a role in MPCs. Furthermore, our data showed that MPC proliferation and muscle regeneration deteriorate more severely as the disease progresses. The mechanisms underlying the decreases in the number of isolated satellite cells and MPC proliferation are

currently unknown. It has been suggested that satellite cells express properly glycosylated α-DG (31) and that myoblasts/MPCs also express properly glycosylated α-DG although its signals are relatively weak compared with those of myotubes (32,33). The basement membrane of skeletal muscle contains DG ligands, laminins and perlecan. It is well established that interactions between the extracellular matrix and cell-surface receptors are involved in cell survival signaling (34). Since it has been proposed that DG-ligand interactions are also involved in cellular signaling mechanisms such as survival and apoptosis pathways (35,36), it is possible that loss of α-DG glycosylation may affect survival signaling regulated by α-DG-basement membrane interaction. In addition, since the Myf5-fukutin-cKO myofibers showed an earlier reduction of fukutin compared with those of MCK-fukutin-cKO, there is a possibility that earlier loss of α-DG glycosylation in myofibers affects disease progression and severity. For example, the absence of α-DG glycosylation during postnatal/juvenile muscle growth and development may have a high impact on muscle degeneration and/or dystrophic pathology in later stages.

As for other muscular dystrophy models with defects in the dystrophin–glycoprotein complex, impaired muscle regeneration has also been reported in *MORE-DG null* mice, in which the DG gene (*Dag1*) is ablated in all cells in the embryo (31), and in older (>1 year) dystrophin-deficient mdx and sarcoglycan-deficient mice (31). The regeneration defects in our Myf5-fukutin-cKO mice appeared at a relatively young age (~3 months), but at this age, Myf5-fukutin-cKO mice already show severe dystrophic pathology. The pathological environment may interfere with efficient muscle regeneration, resulting in decreased regeneration activity as the disease progresses (37). A very recent study also suggested that alterations to the basal lamina microenvironment perturb regeneration potential in dystroglycanopathy (38). Moreover, our data suggest that multiple cycles of degeneration/regeneration may also affect MPC viability, which is consistent with a previous study showing that the progressive exhaustion of functional muscle satellite cells is associated with severe dystrophic phenotype (39). It appears that these disease environments and impaired MPC viability caused by loss of fukutin-dependent modification additively deteriorate regeneration activity, eventually leading to severe and rapid progressive pathology. Together, we conclude that defects in MPC activity contribute to the severe pathology of dystroglycanopathy and propose that dystroglycanopathy is a regeneration-defective disorder.

We observed that some muscle specimens from 16-week-old Myf5-fukutin-cKO mice showed mild phenotype, which was consequently supported by the presence of functionally glycosylated α-DG. Beedle *et al.* (30) also reported that fukutin deletion resulted in moderate to severe muscular dystrophy using Myf5-Cre mice. Because phenotypic variation in our Myf5-fukutin-cKO colony was rarely seen before 12 weeks of age, the variation may be secondary to disease progression. The less phenotypic variation in our colonies could also be due to the number of backcross on C57BL/6 (backcross: more than seven). We speculate that during frequent cycles of muscle degeneration/regeneration, Myf5-independent or less-expressed myogenic cells (40) may be activated and differentiated into myofibers in which the *fukutin* gene escaped Cre-mediated recombination.

Many cases of dystroglycanopathy show the most severe skeletal muscle phenotype, and the severe/typical dystroglycanopathy patients end their short lives without ever standing or walking. Although an increasing number of patients are being diagnosed with dystroglycanopathy worldwide, there have been no therapeutic studies on dystroglycanopathy models after the disease progresses. In this study, for the first time, we succeeded in ameliorating the disease severity in dystroglycanopathy mouse models based on the pathomechanism. It is of importance that limited rescue of fukutin protein in myofibers of Myf5-fukutin-cKO muscles, which have MPC defects, ameliorated the severe phenotype. These data suggest that even after functional and/or substantial loss of MPC occurs, prevention of disease-causing defects in myofibers is a probable therapeutic strategy for muscular dystrophy. Moreover, it is noteworthy that therapeutic effects of the exogenous *fukutin* gene were achieved with relatively lower AAV titers than those used in other gene therapies for structural proteins such as dystrophin and sarcoglycans (41–43). Our results showed that titers that were ~2 orders of magnitude less than those required in previous studies were sufficient to produce a therapeutic effect in Myf5-fukutin-cKO mice. This is consistent with our previous study, which suggested that only a little amount of fukutin is necessary to prevent muscular dystrophy (29). Most dystroglycanopathy genes are identified as glycosyltransferases (11,12,15) or hypothesized to have enzyme-like properties, suggesting that a small amount of exogenous gene would be sufficient for producing therapeutic effects. A small dose of AAV vectors could lower the chances of adverse effects such as immune responses in human (44). In addition, the cDNA sizes of fukutin as well as other dystroglycanopathy genes are suitable for AAV vectors. Taken together, we propose that gene transfer is a promising therapeutic strategy for the amelioration of the severe skeletal muscle pathology of dystroglycanopathy. Human dystroglycanopathy is frequently accompanied by brain and, often, cardiac disorders (1,45). The efficacy of AAV delivery to these affected tissues, timing of administration and therapeutic effects in other fukutin-cKO models should be examined in the future. Although therapeutic interventions that rescue the developmental defects of dystroglycanopathy (such as anomalies in brain structure) are difficult at present, amelioration of the muscle phenotype would be highly beneficial to patients and their families. For example, such treatment might improve patients' physical abilities and postpone the need for respiratory interventions until much later in the course of the disease. Increased physical activity could positively influence both mental development and social interactions. Overall, this study may facilitate future clinical translational research in the field of dystroglycanopathy treatment.

MATERIALS AND METHODS

Generation of fukutin cKO mice

Construction of the targeted allele, establishment of targeted embryonic stem (ES) cells and generation of the chimera

and F1 mice were carried out by Unitech Co. (Kashiwa, Japan). Briefly, exon 2 of mouse *fukutin* was flanked by two loxP sequences (Supplementary Material, Fig. S1A). An Flp recognition target-flanked neo-cassette was inserted upstream of exon 2. The targeting vector was electroporated into C57BL/6 mouse ES cells. Positive clones were selected, and homologous recombination was confirmed by Southern blotting (Supplementary Material, Fig. S1B). The targeted ES cells were injected into blastocysts (BALB/c), and then, chimera mice were bred with C57BL/6 mice to generate founder mice. The founder mice were crossed with the FLPe transgenic mice, producing heterozygous flox mice without the neo-cassette ($fukutin^{lox/+}$). The heterozygous flox mice were intercrossed to obtain homozygous flox mice ($fukutin^{lox/lox}$).

MCK-Cre mice (22) [$MCK\text{-}Cre^{Tg}(+)$, backcrossed for at least 10 generations to C57BL/6] and Myf5-Cre knock-in mice (23) [$Myf5\text{-}Cre^{KI}(+)$] were obtained from The Jackson Laboratory. Myf5-Cre mice were backcrossed for more than six generations to C57BL/6 before crossing with $fukutin^{lox/lox}$ mice. The heterozygous $fukutin^{lox/+}$ carrying MCK-Cre [$fukutin^{lox/+}$:$MCK\text{-}Cre^{Tg}(+)$] or Myf5-Cre [$fukutin^{lox/+}$:$Myf5\text{-}Cre^{KI}(+)$] were then bred with $fukutin^{lox/lox}$ mice to obtain cKO mice. Using this breeding strategy, we obtained the following four genotypes (Supplementary Material, Fig. S1C): for MCK-fukutin-cKO line—[$fukutin^{lox/lox}$:$MCK\text{-}Cre^{Tg}(-)$] (used as WT control), [$fukutin^{lox/lox}$:$MCK\text{-}Cre^{Tg}(+)$] (used as cKO), [$fukutin^{lox/+}$:$MCK\text{-}Cre^{Tg}(+)$] (used as heterozygous control, HET) and [$fukutin^{lox/+}$:$MCK\text{-}Cre^{Tg}(-)$]; and for the Myf5-fukutin-cKO line—[$fukutin^{lox/lox}$:$Myf5\text{-}Cre^{KI}(-)$] (used as WT), [$fukutin^{lox/lox}$:$Myf5\text{-}Cre^{KI}(+)$] (used as cKO), [$fukutin^{lox/+}$:$Myf5\text{-}Cre^{KI}(+)$] (used as HET) and [$fukutin^{lox/+}$:$Myf5\text{-}Cre^{KI}(-)$]. Alternatively, we crossed cKO mice with $fukutin^{lox/lox}$ mice to obtain two genotypes: WT and cKO (Supplementary Material, Fig. S1C). Genotyping was performed using PCR (Supplementary Material, Fig. S1D). Primer sequences and PCR conditions are available on request. Mice were maintained in accordance with the animal care guidelines of Unitech Co. Ltd., Osaka University and Kobe University.

Antibodies

Antibodies used in western blots and immunofluorescence were as follows: mouse monoclonal antibody 8D5 against β-DG (Novacastra); mouse monoclonal antibody IIH6 against glycosylated α-DG (Millipore); goat polyclonal antibody against the C-terminal domain of the α-DG polypeptide (AP-074G-C) (29); goat polyclonal anti-fukutin antibody (106G2) and rabbit polyclonal anti-fukutin antibody (RY213) (5); rat anti-laminin antibody 4H8-2 (Alexis Biochemicals); rabbit polyclonal anti-collagen I antibody (AbD Serotec); and mouse monoclonal anti-embryonic myosin antibody (The Developmental Studies Hybridoma Bank, University of Iowa). A rat monoclonal antibody against the α-DG core protein (3D7-7) was generated using the recombinant α-DG-Fc fusion protein (46); hybridoma clones were selected for reactivity to the C-terminal domain of the α-DG polypeptide. To reduce high background staining of IIH6 in severely affected skeletal muscle sections, commercial IIH6 was labeled with biotin. The IIH6-IgM fractions were prepared from ascites, using protein L-beads (Pierce) and then biotinylated (EZ-Link Micro Sulfo-NHS-Biotinylation Kit; Pierce) according to the manufacturer's instructions.

Preparation of fukutin and DG

Endogenous fukutin was enriched by immunoprecipitation using polyclonal goat anti-fukutin antibody (106G2) from the skeletal muscle lysates. The immunoprecipitated materials were subjected to western blotting using polyclonal rabbit anti-fukutin antibody (RY213). DG from solubilized skeletal muscle was enriched with wheat germ agglutinin-agarose beads (Vector Laboratories) as previously described (29).

Histological and immunofluorescence analyses

For histological and immunofluorescence staining, cryosections (7 μm thick) were prepared. For H&E staining, sections were stained for 2 min in hematoxylin, 1 min in eosin, and then dehydrated with ethanol and xylene. The slides are washed with 0.5% glacial acetic acid, dehydrated and then mounted. For immunofluorescence analysis, sections were treated with cold ethanol/acetic acid (1:1) for 1 min, blocked with 5% goat serum in MOM mouse Ig blocking reagent (Vector Laboratories) at room temperature for 1 h, and then incubated overnight with primary antibodies diluted in MOM diluent (Vector Laboratories) at 4°C. The slides were washed with phosphate-buffered saline (PBS) and incubated with Alexa Fluor 488-conjugated or Alexa Fluor 555-conjugated secondary antibodies (Molecular Probes) at room temperature for 30 min. Sections were observed by fluorescence microscopy (Leica DMR, Leica Microsystems and BZ9000, Keyence). Quantification of the number of Pax7-positive cells and the population of Pax7/MyoD-double-positive cells was performed as previously described (47).

Quantitative and statistical analysis

For quantitative evaluation of muscle pathology, the proportion of myofibers with centrally located nuclei in at least 1000 fibers for each individual was counted. For the evaluation of connective tissue infiltration, the immunofluorescence signal of collagen I was quantitatively measured using the ImageJ software. For the assessment of myofiber size variation, areas of individual myofibers on transverse sections were measured using the ImageJ software. Data represent means with SEM, and P-values ≤ 0.05 were considered statistically significant (Mann–Whitney U test).

Preparation and culture of MPCs

Mononuclear cells from uninjured limb muscles were prepared using 0.2% collagenase type II (Worthington Biochemical) as previously described (28,48). Approximately $3-5 \times 10^6$ or $3-9 \times 10^6$ mononuclear cells from young mice (2-week-old) or adult mice (4-month-old), respectively, were subjected to MPC isolation experiments. Mononuclear cells derived from the skeletal muscles were stained with FITC-conjugated anti-CD31 (Pecam1, Mouse Genome Informatics), anti-CD45

(Ptprc, Mouse Genome Informatics), phycoerythrin-conjugated anti-Sca1 (Ly6a, Mouse Genome Informatics) and biotinylated SM/C-2.6 antibodies (28). Cells were then incubated with 1:400 streptavidin–allophycocyanin (BD Biosciences) on ice for 30 min and resuspended in PBS containing 2% fetal calf serum (FCS) and 2 μg/ml propidium iodide (PI). Cell sorting was performed using an FACS Aria II flow cytometer (BD Immunocytometry Systems). Debris and dead cells were excluded by forward scatter, side scatter and PI gating. Data were collected using the FACSDiva software (BD Biosciences). Myogenic cells from the regenerating muscles were also highly enriched in the SM/C-2.6(+) CD31(−) CD45(−) Sca1(−) cell fraction.

Freshly isolated myogenic cells were cultured in a growth medium of high-glucose Dulbecco's modified Eagle's medium (DMEM-HG; Sigma-Aldrich) containing 20% FCS, 2.5 ng/ml basic fibroblast growth factor (FGF2; PeproTech) and penicillin (100 U/ml)–streptomycin (100 μg/ml) (Gibco BRL) on culture dishes coated with Matrigel (BD Biosciences). Differentiation was induced in a differentiation medium containing DMEM-HG, 5% horse serum and penicillin–streptomycin for 3–4 days. Quantitative analysis for cell proliferation was performed as described previously (47). Fusion index was estimated as the ratio of nuclei in the myotubes to all the nuclei in more than four independent microscopy fields.

CTX experiments

CTX (30 μM; purified from the venom of the snake *Naja nigricollis*; Latoxan) was injected intramuscularly (for young mice, 30 μl to the tibialis anterior and 70 μl to the calf; for adult mice, 50 μl to the tibialis anterior and 100 μl to the calf). Mock injections used only saline solution. The injected muscles were examined 5 or 14 days after the injection. Five days after the injection, areas of individual embryonic myosin-positive fibers were measured (>300 fibers randomly chosen from 5–10 regions per toxin-challenged muscle) in each genotype. Fourteen days after the injection, fiber size variation was quantitatively evaluated by measuring individual laminin-positive fibers (>300 fibers) in each genotype.

AAV gene transfer

To generate *fukutin*-encoding AAV9 vector, the complete open reading frame of mouse *fukutin* gene was cloned into the pAAV-IRES-hrGFP vector (49). The recombinant *fukutin*-encoding AAV9 vector was produced as described previously (49). AAV vectors were injected intramuscularly into the calf and tibialis anterior (at 1 week to the tibialis anterior, $0.8–1.6 \times 10^9$ vector genome in saline solution; at 1 week to the calf or at 8 weeks to the tibialis anterior, $2–4 \times 10^9$ vector genome; and at 8 weeks to the calf, $4–8 \times 10^9$ vector genome). For tail vein injections and intraperitoneal injections, $\sim 2 \times 10^{10}$ and $\sim 1 \times 10^{10}$ vector genome was used, respectively.

Miscellaneous

For western blotting, the proteins were separated using 4–15% linear gradient SDS–PAGE (Bio-Rad). Gels were transferred to polyvinylidene fluoride membrane (Millipore). Blots were developed by horseradish peroxidase-enhanced chemiluminescence (Supersignal West Pico, Pierce; or ECL Plus, GE Healthcare). Laminin-binding activity was determined by the laminin overlay assay as described previously (29). Serum CK activity was measured using the CPK kit (WAKO). For Evans blue dye uptake, Evans blue dye (10 mg/ml in saline) was intraperitoneally injected (100 μl/10 g of body weight). After 5 h, the mice were made to exercise on a downhill (15°) treadmill for 60 min (MK-680S, Muromachi Kikai). Twenty-four hours after the exercise, frozen tissue samples were prepared. Serum was prepared before 24 h and after 2 h of the exercise. Grip strength was measured for 10 consecutive trials for each mouse, using a strength meter (Ohara Ika Sangyo Co. Ltd, Tokyo), and 20% of the top and the bottom values were excluded to obtain the mean value.

SUPPLEMENTARY MATERIAL

Supplementary Material is available at *HMG* online.

ACKNOWLEDGEMENTS

We would like to thank the past and present members of T.T.'s laboratory for fruitful discussions and scientific contributions. We also thank Hiromi Hayashita-Kinoh for providing technical support.

Conflict of Interest statement. None declared.

FUNDING

This work was supported by the Ministry of Health, Labor and Welfare of Japan [Intramural Research Grant for Neurological and Psychiatric Disorders of National Center of Neurology and Psychiatry (23B-5)], the Ministry of Education, Culture, Sports, Science and Technology of Japan [a Grant-in-Aid for Scientific Research (A) 23249049 to T.T., a Grant-in-Aid for Young Scientists (A) 24687017 to M.K. and a Grant-in-Aid for Scientific Research on Innovative Areas (No. 23110002, Deciphering Sugar Chain-based Signals Regulating Integrative Neuronal Functions) 24110508 to M.K.], a Senri Life Science Foundation grant to M.K., a Takeda Science Foundation grant to M.K. and a Naito Foundation grant to M.K.

REFERENCES

1. Godfrey, C., Foley, A.R., Clement, E. and Muntoni, F. (2011) Dystroglycanopathies: coming into focus. *Curr. Opin. Genet. Dev.*, **21**, 278–285.
2. Hayashi, Y.K., Ogawa, M., Tagawa, K., Noguchi, S., Ishihara, T., Nonaka, I. and Arahata, K. (2001) Selective deficiency of alpha-dystroglycan in Fukuyama-type congenital muscular dystrophy. *Neurology*, **57**, 115–121.
3. Michele, D.E., Barresi, R., Kanagawa, M., Saito, F., Cohn, R.D., Satz, J.S., Dollar, J., Nishino, I., Kelley, R.I., Somer, H. *et al.* (2002) Post-translational disruption of dystroglycan-ligand interactions in congenital muscular dystrophies. *Nature*, **418**, 417–422.
4. Kobayashi, K., Nakahori, Y., Miyake, M., Matsumura, K., Kondo-Iida, E., Nomura, Y., Segawa, M., Yoshioka, M., Saito, K., Osawa, M. *et al.* (1998) An ancient retrotransposal insertion causes Fukuyama-type congenital muscular dystrophy. *Nature*, **394**, 388–392.

5. Taniguchi-Ikeda, M., Kobayashi, K., Kanagawa, M., Yu, C.C., Mori, K., Oda, T., Kuga, A., Kurahashi, H., Akman, H.O., DiMauro, S. *et al.* (2011) Pathogenic exon-trapping by SVA retrotransposon and rescue in Fukuyama muscular dystrophy. *Nature*, **478**, 127–131.
6. Fukuyama, Y., Osawa, M. and Suzuki, H. (1981) Congenital progressive muscular dystrophy of the Fukuyama type-clinical, genetic and pathological considerations. *Brain Dev.*, **3**, 1–29.
7. Godfrey, C., Clement, E., Mein, R., Brockington, M., Smith, J., Talim, B., Straub, V., Robb, S., Quinlivan, R., Feng, L. *et al.* (2007) Refining genotype phenotype correlations in muscular dystrophies with defective glycosylation of dystroglycan. *Brain*, **130**, 2725–2735.
8. Tachikawa, M., Kanagawa, M., Yu, C.C., Kobayashi, K. and Toda, T. (2012) Mislocalization of fukutin protein by disease-causing missense mutations can be rescued with treatments directed at folding amelioration. *J. Biol. Chem.*, **287**, 8398–8406.
9. Wells, L. (2013) The O-mannosylation pathway: glycosyltransferases and proteins implicated in congenital muscular dystrophy. *J. Biol. Chem.*, **288**, 6930–6935.
10. Buysse, K., Riemersma, M., Powell, G., van Reeuwijk, J., Chitayat, D., Roscioli, T., Kamsteeg, E.J., van den Elzen, C., van Beusekom, E., Blaser, S. *et al.* (2013) Missense mutations in β-1,3-*N*-acetylglucosaminyltransferase 1 (B3GNT1) cause Walker-Warburg syndrome. *Hum. Mol. Genet.*, **22**, 1746–1754.
11. Manya, H., Chiba, A., Yoshida, A., Wang, X., Chiba, Y., Jigami, Y., Margolis, R.U. and Endo, T. (2004) Demonstration of mammalian protein *O*-mannosyltransferase activity: coexpression of POMT1 and POMT2 required for enzymatic activity. *Proc. Natl Acad. Sci. USA*, **101**, 500–505.
12. Yoshida, A., Kobayashi, K., Manya, H., Taniguchi, K., Kano, H., Mizuno, M., Inazu, T., Mitsuhashi, H., Takahashi, S., Takeuchi, M. *et al.* (2001) Muscular dystrophy and neuronal migration disorder caused by mutations in a glycosyltransferase, POMGnT1. *Dev. Cell*, **1**, 717–724.
13. Yoshida-Moriguchi, T., Yu, L., Stalnaker, S.H., Davis, S., Kunz, S., Madson, M., Oldstone, M.B., Schachter, H., Wells, L. and Campbell, K.P. (2010) *O*-mannosyl phosphorylation of alpha-dystroglycan is required for laminin binding. *Science*, **327**, 88–92.
14. Kuga, A., Kanagawa, M., Sudo, A., Chan, Y.M., Tajiri, M., Manya, H., Kikkawa, Y., Nomizu, M., Kobayashi, K., Endo, T. *et al.* (2012) Absence of post-phosphoryl modification in dystroglycanopathy mouse models and wild-type tissues expressing non-laminin binding form of α-dystroglycan. *J. Biol. Chem.*, **287**, 9560–9567.
15. Inamori, K., Yoshida-Moriguchi, T., Hara, Y., Anderson, M.E., Yu, L. and Campbell, K.P. (2012) Dystroglycan function requires xylosyl- and glucuronyltransferase activities of LARGE. *Science*, **335**, 93–96.
16. Ibraghimov-Beskrovnaya, O., Ervasti, J.M., Leveille, C.J., Slaughter, C.A., Sernett, S.W. and Campbell, K.P. (1992) Primary structure of dystrophin-associated glycoproteins linking dystrophin to the extracellular matrix. *Nature*, **355**, 696–702.
17. Barresi, R. and Campbell, K.P. (2006) Dystroglycan: from biosynthesis to pathogenesis of human disease. *J. Cell Sci.*, **119**, 199–207.
18. Taniguchi, M., Kurahashi, H., Noguchi, S., Fukudome, T., Okinaga, T., Tsukahara, T., Tajima, Y., Ozono, K., Nishino, I., Nonaka, I. and Toda, T. (2006) Aberrant neuromuscular junctions and delayed terminal muscle fiber maturation in alpha-dystroglycanopathies. *Hum. Mol. Genet.*, **15**, 1279–1289.
19. Hara, Y., Balci-Hayta, B., Yoshida-Moriguchi, T., Kanagawa, M., Beltrán-Valero de Bernabé, D., Gündeşli, H., Willer, T., Satz, J.S., Crawford, R.W., Burden, S.J. *et al.* (2011) A dystroglycan mutation associated with limb-girdle muscular dystrophy. *N. Engl. J. Med.*, **364**, 939–946.
20. Roscioli, T., Kamsteeg, E.J., Buysse, K., Maystadt, I., van Reeuwijk, J., van den Elzen, C., van Beusekom, E., Riemersma, M., Pfundt, R., Vissers, L.E. *et al.* (2012) Mutations in ISPD cause Walker-Warburg syndrome and defective glycosylation of α-dystroglycan. *Nat. Genet.*, **44**, 581–585.
21. Willer, T., Lee, H., Lommel, M., Yoshida-Moriguchi, T., de Bernabe, D.B., Venzke, D., Cirak, S., Schachter, H., Vajsar, J., Voit, T. *et al.* (2012) ISPD loss-of-function mutations disrupt dystroglycan O-mannosylation and cause Walker-Warburg syndrome. *Nat. Genet.*, **44**, 575–580.
22. Brüning, J.C., Michael, M.D., Winnay, J.N., Hayashi, T., Hörsch, D., Accili, D., Goodyear, L.J. and Kahn, C.R. (1998) A muscle-specific insulin receptor knockout exhibits features of the metabolic syndrome of NIDDM without altering glucose tolerance. *Mol. Cell*, **2**, 559–569.
23. Tallquist, M.D., Weismann, K.E., Hellström, M. and Soriano, P. (2000) Early myotome specification regulates PDGFA expression and axial skeleton development. *Development*, **127**, 5059–5070.
24. Lyons, G.E., Mühlebach, S., Moser, A., Masood, R., Paterson, B.M., Buckingham, M.E. and Perriard, J.C. (1991) Developmental regulation of creatine kinase gene expression by myogenic factors in embryonic mouse and chick skeletal muscle. *Development*, **113**, 1017–1029.
25. Trask, R.V. and Billadello, J.J. (1990) Tissue-specific distribution and developmental regulation of M and B creatine kinase mRNAs. *Biochim. Biophys. Acta*, **1049**, 182–188.
26. Vilquin, J.T., Brussee, V., Asselin, I., Kinoshita, I., Gingras, M. and Tremblay, J.P. (1998) Evidence of mdx mouse skeletal muscle fragility in vivo by eccentric running exercise. *Muscle Nerve*, **21**, 567–576.
27. Durbeej, M., Sawatzki, S.M., Barresi, R., Schmainda, K.M., Allamand, V., Michele, D.E. and Campbell, K.P. (2003) Gene transfer establishes primacy of striated vs. smooth muscle sarcoglycan complex in limb-girdle muscular dystrophy. *Proc. Natl Acad. Sci. USA*, **100**, 8910–8915.
28. Fukada, S., Higuchi, S., Segawa, M., Koda, K., Yamamoto, Y., Tsujikawa, K., Kohama, Y., Uezumi, A., Imamura, M., Miyagoe-Suzuki, Y. *et al.* (2004) Purification and cell-surface marker characterization of quiescent satellite cells from murine skeletal muscle by a novel monoclonal antibody. *Exp. Cell Res.*, **296**, 245–255.
29. Kanagawa, M., Nishimoto, A., Chiyonobu, T., Takeda, S., Miyagoe-Suzuki, Y., Wang, F., Fujikake, N., Taniguchi, M., Lu, Z., Tachikawa, M. *et al.* (2009) Residual laminin-binding activity and enhanced dystroglycan glycosylation by LARGE in novel model mice to dystroglycanopathy. *Hum. Mol. Genet.*, **18**, 621–631.
30. Beedle, A.M., Turner, A.J., Saito, Y., Lueck, J.D., Foltz, S.J., Fortunato, M.J., Nienaber, P.M. and Campbell, K.P. (2012) Mouse fukutin deletion impairs dystroglycan processing and recapitulates muscular dystrophy. *J. Clin. Invest.*, **122**, 3330–3342.
31. Cohn, R.D., Henry, M.D., Michele, D.E., Barresi, R., Saito, F., Moore, S.A., Flanagan, J.D., Skwarchuk, M.W., Robbins, M.E., Mendell, J.R., Williamson, R.A. and Campbell, K.P. (2002) Disruption of DAG1 in differentiated skeletal muscle reveals a role for dystroglycan in muscle regeneration. *Cell*, **110**, 639–648.
32. Barresi, R., Michele, D.E., Kanagawa, M., Harper, H.A., Dovico, S.A., Satz, J.S., Moore, S.A., Zhang, W., Schachter, H., Dumanski, J.P. *et al.* (2004) LARGE can functionally bypass alpha-dystroglycan glycosylation defects in distinct congenital muscular dystrophies. *Nat. Med.*, **10**, 696–703.
33. Hara, Y., Kanagawa, M., Kunz, S., Yoshida-Moriguchi, T., Satz, J.S., Kobayashi, Y.M., Zhu, Z., Burden, S.J., Oldstone, M.B. and Campbell, K.P. (2011) Like-acetylglucosaminyltransferase (LARGE)-dependent modification of dystroglycan at Thr-317/319 is required for laminin binding and arenavirus infection. *Proc. Natl Acad. Sci. USA*, **108**, 17426–17431.
34. Gilmore, A.P. (2005) Anoikis. *Cell Death Differ.*, **12**, 1473–1477.
35. Langenbach, K.J. and Rando, T.A. (2002) Inhibition of dystroglycan binding to laminin disrupts the PI3K/AKT pathway and survival signaling in muscle cells. *Muscle Nerve*, **26**, 644–653.
36. Munoz, J., Zhou, Y. and Jarrett, H.W. (2010) LG4-5 domains of laminin-211 binds alpha-dystroglycan to allow myotube attachment and prevent anoikis. *J. Cell. Physiol.*, **222**, 111–119.
37. Morgan, J.E. and Zammit, P.S. (2010) Direct effects of the pathogenic mutation on satellite cell function in muscular dystrophy. *Exp. Cell Res.*, **316**, 3100–3108.
38. Ross, J., Benn, A., Jonuschies, J., Boldrin, L., Muntoni, F., Hewitt, J.E., Brown, S.C. and Morgan, J.E. (2012) Defects in glycosylation impair satellite stem cell function and niche composition in the muscles of the dystrophic Large(myd) mouse. *Stem Cells*, doi: 10.1002/stem.1197.
39. Sacco, A., Mourkioti, F., Tran, R., Choi, J., Llewellyn, M., Kraft, P., Shkreli, M., Delp, S., Pomerantz, J.H., Artandi, S.E. and Blau, H.M. (2010) Short telomeres and stem cell exhaustion model Duchenne muscular dystrophy in mdx/mTR mice. *Cell*, **143**, 1059–1071.
40. Gensch, N., Borchardt, T., Schneider, A., Riethmacher, D. and Braun, T. (2008) Different autonomous myogenic cell populations revealed by ablation of Myf5-expressing cells during mouse embryogenesis. *Development*, **135**, 1597–1604.
41. Gregorevic, P., Allen, J.M., Minami, E., Blankinship, M.J., Haraguchi, M., Meuse, L., Finn, E., Adams, M.E., Froehner, S.C., Murry, C.E. and Chamberlain, J.S. (2006) rAAV6-Microdystrophin preserves muscle

function and extends lifespan in severely dystrophic mice. *Nat. Med.*, **12**, 787–789.
42. Yoshimura, M., Sakamoto, M., Ikemoto, M., Mochizuki, Y., Yuasa, K., Miyagoe-Suzuki, Y. and Takeda, S. (2004) AAV vector-mediated microdystrophin expression in a relatively small percentage of mdx myofibers improved the mdx phenotype. *Mol. Ther.*, **10**, 821–828.
43. Pacak, C.A., Walter, G.A., Gaidosh, G., Bryant, N., Lewis, M.A., Germain, S., Mah, C.S., Campbell, K.P. and Byrne, B.J. (2007) Long-term skeletal muscle protection after gene transfer in a mouse model of LGMD-2D. *Mol. Ther.*, **15**, 1775–1781.
44. Nathwani, A.C., Tuddenham, E.G., Rangarajan, S., Rosales, C., McIntosh, J., Linch, D.C., Chowdary, P., Riddell, A., Pie, A.J., Harrington, C. *et al.* (2011) Adenovirus-associated virus vector-mediated gene transfer in hemophilia B. *N. Engl. J. Med.*, **365**, 2357–2365.
45. Pane, M., Messina, S., Vasco, G., Foley, A.R., Morandi, L., Pegoraro, E., Mongini, T., D'Amico, A., Bianco, F., Lombardo, M.E. *et al.* (2012) Respiratory and cardiac function in congenital muscular dystrophies with alpha dystroglycan deficiency. *Neuromuscul. Disord.*, **22**, 685–689.
46. Kanagawa, M., Omori, Y., Sato, S., Kobayashi, K., Miyagoe-Suzuki, Y., Takeda, S., Endo, T., Furukawa, T. and Toda, T. (2010) Post-translational maturation of dystroglycan is necessary for pikachurin binding and ribbon synaptic localization. *J. Biol. Chem.*, **285**, 31208–31216.
47. Fukada, S., Yamaguchi, M., Kokubo, H., Ogawa, R., Uezumi, A., Yoneda, T., Matev, M.M., Motohashi, N., Ito, T., Zolkiewska, A. *et al.* (2011) Hesr1 and Hesr3 are essential to generate undifferentiated quiescent satellite cells and to maintain satellite cell numbers. *Development*, **138**, 4609–4619.
48. Segawa, M., Fukada, S., Yamamoto, Y., Yahagi, H., Kanematsu, M., Sato, M., Ito, T., Uezumi, A., Hayashi, S., Miyagoe-Suzuki, Y. *et al.* (2008) Suppression of macrophage functions impairs skeletal muscle regeneration with severe fibrosis. *Exp. Cell Res.*, **314**, 3232–3244.
49. Shin, J.H., Nitahara-Kasahara, Y., Hayashita-Kinoh, H., Ohshima-Hosoyama, S., Kinoshita, K., Chiyo, T., Okada, H., Okada, T. and Takeda, S. (2011) Improvement of cardiac fibrosis in dystrophic mice by rAAV9-mediated microdystrophin transduction. *Gene Ther.*, **18**, 910–919.

ORIGINAL ARTICLE

Mutations in *COQ2* in Familial and Sporadic Multiple-System Atrophy

The Multiple-System Atrophy Research Collaboration

ABSTRACT

BACKGROUND

Multiple-system atrophy is an intractable neurodegenerative disease characterized by autonomic failure in addition to various combinations of parkinsonism, cerebellar ataxia, and pyramidal dysfunction. Although multiple-system atrophy is widely considered to be a nongenetic disorder, we previously identified multiplex families with this disease, which indicates the involvement of genetic components.

METHODS

In combination with linkage analysis, we performed whole-genome sequencing of a sample obtained from a member of a multiplex family in whom multiple-system atrophy had been diagnosed on autopsy. We also performed mutational analysis of samples from members of five other multiplex families and from a Japanese series (363 patients and two sets of controls, one of 520 persons and one of 2383 persons), a European series (223 patients and 315 controls), and a North American series (172 patients and 294 controls). On the basis of these analyses, we used a yeast complementation assay and measured enzyme activity of parahydroxybenzoate-polyprenyl transferase. This enzyme is encoded by the gene *COQ2* and is essential for the biosynthesis of coenzyme Q_{10}. Levels of coenzyme Q_{10} in lymphoblastoid cells and brain tissue were measured on high-performance liquid chromatography.

RESULTS

We identified a homozygous mutation (M128V-V393A/M128V-V393A) and compound heterozygous mutations (R387X/V393A) in *COQ2* in two multiplex families. Furthermore, we found that a common variant (V393A) and multiple rare variants in *COQ2*, all of which are functionally impaired, are associated with sporadic multiple-system atrophy. The V393A variant was exclusively observed in the Japanese population.

CONCLUSIONS

Functionally impaired variants of *COQ2* were associated with an increased risk of multiple-system atrophy in multiplex families and patients with sporadic disease, providing evidence of a role of impaired COQ2 activities in the pathogenesis of this disease. (Funded by the Japan Society for the Promotion of Science and others.)

The members of the Multiple-System Atrophy Research Collaboration are listed in the Appendix. Address reprint requests to Dr. Shoji Tsuji, Department of Neurology, University of Tokyo, 7-3-1 Hongo, Bunkyo-ku, Tokyo 113-8655, Japan, or at tsuji@m.u-tokyo.ac.jp.

This article was published on June 12, 2013, and updated on July 3, 2014, at NEJM.org.

N Engl J Med 2013;369:233-44.
DOI: 10.1056/NEJMoa1212115

Multiple-system atrophy is a progressive neurodegenerative disease that is clinically characterized by autonomic failure in addition to various combinations of parkinsonism, cerebellar ataxia, and pyramidal dysfunction. The term multiple-system atrophy was introduced in 1969 to encompass the disease entities of olivopontocerebellar ataxia, striatonigral degeneration, and the Shy–Drager syndrome, on the basis of neuropathological findings in these disorders.[1] Multiple-system atrophy is characterized by the development of cytoplasmic aggregates of α-synuclein, primarily in oligodendroglia.[2-7] However, the pathogenic mechanisms underlying this disease remain unknown, making it difficult to develop effective therapies.

The disorder is classified into two subtypes: subtype C, characterized predominantly by cerebellar ataxia, and subtype P, characterized predominantly by parkinsonism.[8] Among patients with multiple-system atrophy, subtype C has been reported to be more prevalent than subtype P in the Japanese population (65 to 67% vs. 33 to 35%),[9,10] whereas subtype P has been reported to be more prevalent than subtype C in Europe (63% vs. 34%)[11] and North America (60% vs. 13%, with 27% of cases unclassified).[12] Although multiple-system atrophy has been defined as a nongenetic disorder until recently, several multiplex families with the disease have been described, indicating that strong genetic factors confer susceptibility to the disease.[13-15]

METHODS

PATIENTS AND MULTIPLEX FAMILIES

Patients with multiple-system atrophy were enrolled in the study on the basis of research protocols that were approved by the institutional review board at each participating center. Written informed consent was obtained from all participants.

The diagnosis of multiple-system atrophy was made on the basis of the current consensus criteria for the disease.[8] Four Japanese families (Families 1 through 4, whose members have been described previously[13]) and two additional Japanese families (Family 8 and Family 12) were enrolled in this study (Fig. 1). In Family 1, the parents were first-degree cousins, which is consistent with autosomal recessive inheritance. The clinical features of these families are summarized in Table S1 in the Supplementary Appendix, available with the full text of this article at NEJM.org.

Autopsy findings for Participants II-4[13] and II-8 in Family 1 and Participant II-6 in Family 8 showed widespread and abundant cytoplasmic aggregates of α-synuclein, primarily in oligodendroglia, in association with neurodegeneration in striatonigral and olivopontocerebellar structures. These findings confirmed the diagnosis of multiple-system atrophy.

PATIENTS WITH SPORADIC DISEASE AND CONTROLS

As with the multiplex families, the diagnosis of sporadic multiple-system atrophy was made on the basis of the current consensus criteria.[8] A total of 363 patients with multiple-system atrophy and 520 controls were included in the Japanese series, 223 patients and 315 controls in the European series, and 172 patients and 294 controls in the North American series (persons of European or Hispanic descent living in North America) (Text S2 and Table S2 in the Supplementary Appendix). Ancestry was determined by self-report on a multiple-choice questionnaire. We also enrolled an independent series of 2383 Japanese controls.

ASSOCIATION WITH OTHER NEURODEGENERATIVE DISEASES

To determine the specificity of the association between variants in candidate genes and multiple-system atrophy, we enrolled 2728 Japanese patients with Alzheimer's disease, 659 with Parkinson's disease, and 634 with amyotrophic lateral sclerosis (ALS). Their demographic characteristics are provided in Text S2 in the Supplementary Appendix.

LINKAGE ANALYSIS AND WHOLE-GENOME SEQUENCING

We performed parametric and nonparametric linkage analyses using Affymetrix SNP 6.0 arrays and software for linkage analysis.[16,17] The genomic DNA from Participant II-4 in Family 1 was subjected to four runs in an Illumina Genome Analyzer IIx (100-bp-long paired ends). We used BWA software[18] and SAMtools sequence-alignment mapping[19] with the default settings for alignment and variation detection against the human reference genome (National Center for Biotechnology Information build 36 [also known as hg18]).